OPTIMIZATION OF PIGMENTED COATINGS FOR CONCENTRATING SOLAR THERMAL APPLICATIONS

By
Refet Ali Yalçın
B.S, in Mechanical Engineering, Middle East Technical University, 2009

Submitted to the Institute for Graduate Studies in
Science and Engineering in partial fulfillment of
The requirements for the degree of
Master of Science

Graduate Program in Mechanical Engineering
Boğaziçi University
2012

ACKNOWLEDGEMENTS

I would like to express sincere gratitude to my thesis supervisor Hakan Ertürk for his academic support, motivation and the kind guidance he has shown throughout the study.

I would like to thank my mother Zozan, my brother Ömer and my friend Ümit Altunyurt for their endless support and finding ways to encourage me for accomplishing my thesis.

This thesis has been supported by Bogazici University under B.U. Research Fund AP-5566P.

ABSTRACT

OPTIMIZATION OF PIGMENTED COATINGS FOR CONCENTRATING SOLAR THERMAL APPLICATIONS

Spectrally selective coatings are used in absorbers of solar collectors to maximize efficiency of solar thermal energy systems. Desired coating should have high absorptance at solar wavelengths and low emittance at the wavelengths where absorber emits heat. This study focuses on pigmented coatings that consist of a binder and uniformly distributed nano-particles known as pigments that exhibit the desired spectrally selective behavior. Radiative behavior of coatings depends on coating thickness, pigment size, concentration, and the optical properties of binder and pigment materials. In order to understand the effect of these parameters, a unified radiative model of the pigmented coatings is developed, Lorentz-Mie theory in conjunction with Hartel theory to incorporate the multiple scattering effects is used to predict radiation properties for independent scattering, T-Matrix method is used to incorporate the dependent scattering and effective medium theory is used to handle cases with very small pigments. Through the solution of the radiative transfer equation by the four flux method, spectral reflectance is predicted. Design of such a coating is formulated as an inverse problem of estimating design variables such as pigment size, concentration and material to yield the desired spectral emittance of the ideal coating. The nonlinear problem is solved by optimization applying two methods; the Quasi Newton method and Nelder Mead simplex algorithm. While both algorithms are capable of providing the same solution, the convergence of Quasi Newton method is found to be superior to that of Nelder Mead simplex algorithm.

ÖZET

YOĞUNLAŞTIRICILI ISIL GÜNEŞ UYGULAMALARINDA KULLANILAN PİGMENTLİ BOYALARIN OPTİMİZASYONU

Isıl güneş enerji sistemlerindeki kollektörlerin verimliliğini üst düzeye çıkartmak için ışık tayfına göre seçici davranan boyalar kullanılır. Bu amaçla kullanılacak ideal bir boya; güneşin ışınım yaptığı dalga boylarında yüksek soğurum özelliğine, kollektörün ışınım yaptığı dalgaboylarında ise düşük ışıma özelliğine sahip olmalıdır. Bu çalışma; dalga boyuna gore seçicil davranış gösteren ve bir çözücünün içerisinde tekdüze şekilde bulunan, nanometre boyutunda parçacıklar ile ilgilidir. Boyaların ışıma davranışları boyanın kalınlığına, pigmentlerinin çapına, konstantrasyonuna ve pigment ile çözücünün optik özelliklerine bağlıdır. Bu parametrelerin etkisini anlamak için, pigmentli boyaların birleştirilmiş bir modeli oluşturuldu. Bu modeli oluştururken bağımsız çoklu saçılımları modellemek için Hartel teorisi ile birlikle Lorentz-Mie teorisi, bağımlı saçılımları modellemek için T-Matrix metodu, çok küçük pigmentleri modellemek için ise etkin ortam teorisi kullanıldı. Işınım transferi denklemini çözmek böylece dalgaboyuna bağlı yansımayı bulmak için ise dört akı metodu kullanıldı. Bu boyanın tasarımı, ideal boyanın istenen dalgaboyuna bağlı ışımasını verecek şekilde parçacık boyu ve konsantrasyonu gibi parametlere bağlı şekilde, ters problem olarak formüle edildi. Quasi-Newton metodu ve Nelder Mead simplex algoritması kullanılarak, lineer olmayan bu problem optimizasyon yapılarak çözüldü. Her iki algoritma benzer sonuca ulaşsa da, Quasi Newton metodunun Nelder Mead'den daha kısa sürede sonuca ulaştığı görüldü.

TABLE OF CONTENTS

LIST OF FIGURES

LIST OF TABLES

LIST OF SYMBOLS

$_1$	Pigment material
$_2$	Matrix material
$A_1,..,A_5$	Constants for four flux method
a_n, b_n	Mie coefficients
$\mathbf{B}^k$	Inverse of approximation to Hessian matrix at k-th iteration
$C_0,..,C_2$	Constants for four flux method
C_f	Concentration factor of the concentrating solar collector
$C_{ext,\lambda}$	Extinction cross section [nm]
$C_{sca,\lambda}$	Scattering cross section [nm]
$_c$	collimated
$_d$	diffuse
$E_{b,\lambda}$	Spectral blackbody emissive power [W/m^2-μm]
$G_{s,\lambda}$	Spectral solar irradiance [W/m^2-μm]
$\mathbf{H}^k$	Hessian matrix at k-th iteration
$I_{c,\lambda}$	Collimated spectral intensity in +z direction [W/m^2-μm-sr]
$I_{d,\lambda}$	Diffuse spectral intensity in +z direction [W/m^2-μm-sr]
$J_{c,\lambda}$	Collimated spectral intensity in -z direction [W/m^2-μm-sr]
$J_{d,\lambda}$	Diffuse spectral intensity in -z direction [W/m^2-μm-sr]
$F(\chi)$	Objective funct`ion to be minimized
f_v	Pigment volume fraction
k	Extinction index of material
m	Relative complex refractive index of material
n	Refractive index of material
$p(\mu)$	Scattering phase function
$\mathbf{p}^k$	Direction of search step at k-th iteration
r_c	Boundary reflectivity for the collimated intensity from outside to coating
r_c'	Boundary reflectivity for the collimated intensity from substrate to coating
r_d	Boundary reflectivity for the diffuse intensity from coating to outside
r_d'	Boundary reflectivity for the diffuse intensity from coating to substrate

r_p	Pigment radius [nm]
R_λ	Spectral reflectance
q''	Absorber net heat flux [W/m^2]
t	Thickness of the coating [nm]
T_a	Absorber temperature [K]
x	Size parameter
V	Volume [nm^3]
α_λ	Spectral absorptance
β_λ	Spectral extinction coefficient [1/m]
γ^k	Search step size at k-th iteration
ε_λ	Spectral emittance
θ	Polar angle
$_\lambda$	Spectral quantity
μ	$cos(\theta)$
ξ	Average pathlength parameter
σ_c	Forward scattering ratio for the collimated intensity
σ_d	Forward scattering ratio for the diffuse intensity
$\sigma_{s,\lambda}$	Spectral scattering coefficient [1/m]
χ	Unknown vector

1. INTRODUCTION

1.1. Motivation

Energy is driving force of civilizations and production of energy has been one of the major interests of engineers throughout history. Energy consumption has been increasing and world's current energy consumption is 11165 million tones oil equivalent per year (Bilim ve Teknik, 2011) that is obtained from different sources. Major energy sources can be classified as fossil, nuclear, renewable and biofuels, utilization of each source has its advantages and disadvantages.

Fossil fuels such as oil, coal and natural gas have been the most widely used energy source since the industrial revolution. Although use of other resources have been increasing in the recent decades, the ratio of the energy produced by fossil fuels to the total energy produced is about 85% as shown in Figure 1.1. It is relatively easier to utilize and transport fossil fuels and their low cost per kilowatt hour as presented in Figure 1.2 is the major reason behind their popularity.

Relying predominantly on fossil fuels for global energy demand leads to economical, political, and environmental problems, although known reserves are enough for 40 years for oil and 60 years for gas at current consumption rates (Vidal, 2005). Increasing demand on a limited resource leads to an increase in energy prices that is a major concern for global economy. Moreover, many political problems and conflicts have been arising as controlling energy resources is an important concern for all states. Besides all these, utilizing fossil fuels causes serious environmental problems. There have been many incidents such as the disaster in Gulf of Mexico in 2009 that have proven that acquiring fossil fuels have serious impact on nature and ecosystem. Extended fossil fuel consumption causes an increase of CO_2 and other combustion gases such as soot and NO_x concentration in the atmosphere. As these gases are radiatively participating that contribute to the greenhouse effect, significant increases in the concentration of these gases leads to global climate change.

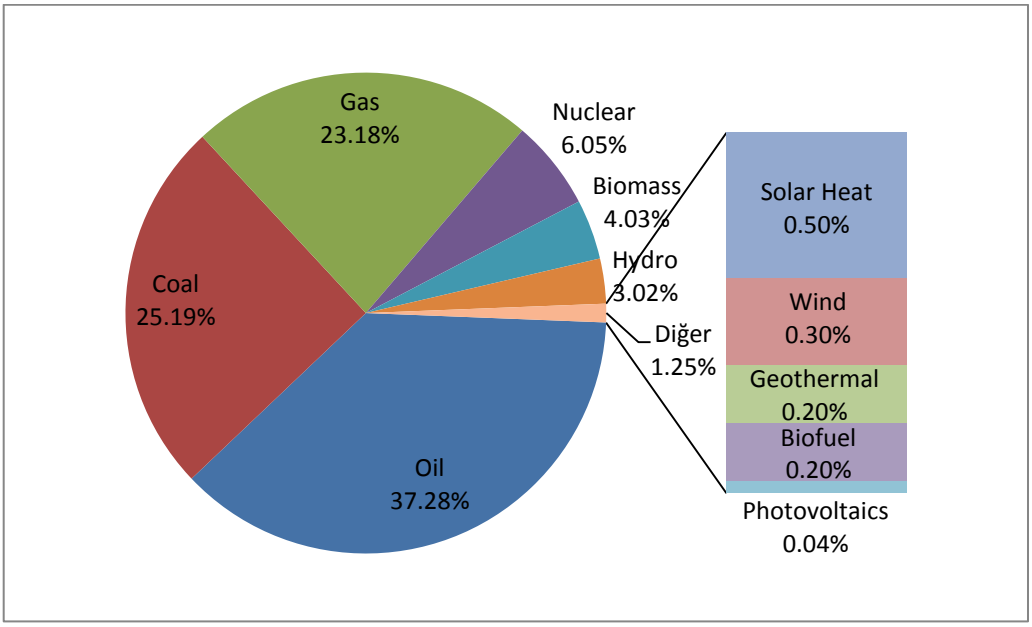

Figure 1.1. Global energy usage in 2005 (British Petroleum, 2006) (Renewables Global Status Report, 2006).

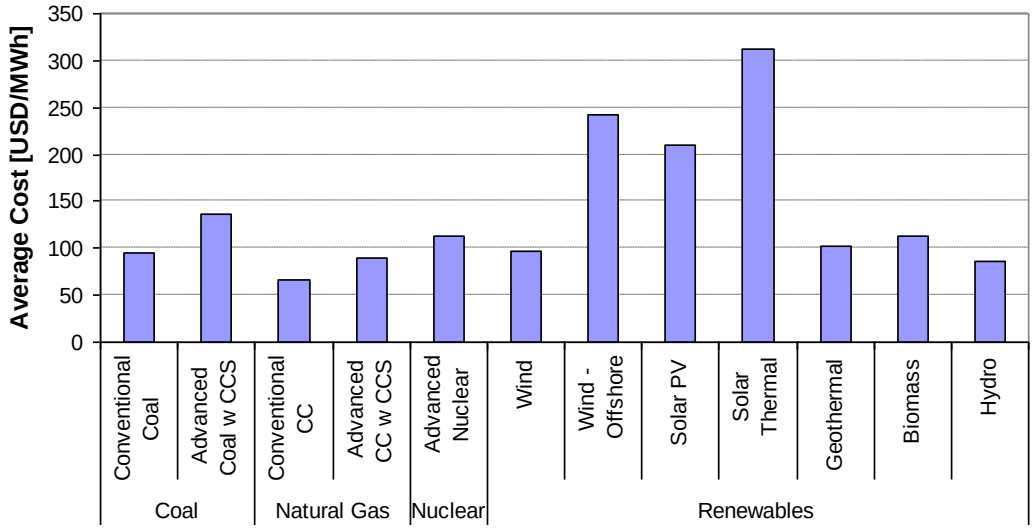

Figure 1.2. Variation in levelized cost of resources (Energy Information Administration, 2010).

Biomass is a carbon, oxygen and hydrogen based renewable energy source. It is the oldest energy source and has a wide variety such as wood, municipal solid waste, landfill gases, alcohol fuel. Total biomass energy utilized in U.S was 11353 MW in 2009. 4405 MW of this power was from waste such as landfill gases and municipal solid waste while

the rest is from wood and derived fuels. As well as it is used directly, biomass can also be converted into biofuel which is widely used in Europe.

Being both portable any easily combusting, biofuels became a good alternative to fossil fuels. Bioalcohol and biodiesel are mostly used biofuel types, by fermentation of glucose derived from products such as wheat and corn. Ethanol fuel is produced. Similarly by transesterification process, biodiesel, which is used in many European countries, is produced from fats and oils.

The leading alternative energy source is nuclear energy as shown in Figure 1.1. Although nuclear power plants do not emit carbon dioxide or any other greenhouse gases, safety concerns in regards to gamma radiation leaks are high. Many scientists and engineers argue that risk of accidents are very low; however, any accident causes significant destructions to human health, economy and ecology as it could be remembered from Fukushima Daiichi and Chernobyl nuclear disasters in 2011 and 1986 respectively. Another significant concern is nuclear waste management and there has not been a widely accepted solution for this problem.

All these concerns and problems have increased interest on utilization of renewable energy sources. Hydro-systems, solar energy, geothermal sources and wind are main renewable energy sources. Although the environmental issues might be resolved through utilization of renewable energy sources, it must be noted that utilization of some renewable energy sources also have significant environmental impacts. Hydroelectric energy systems utilizing the potential energy of a water source is the most commonly used renewable energy. However, it is well known that hydroelectric systems have significant impact on natural ecosystem, and furthermore leads to greenhouse effect where the dead plants in water lead to significant methane emissions.

Geothermal, wind and solar energy systems are environmentally friendly energy systems unlike the hydro-power systems. Geothermal energy is only available at limited regions and generally it is used for domestic house heating as outlet temperature is not feasible to produce electricity. Similar to geothermal energy, wind energy is available at limited regions and also wind farms create noise pollution and create unpleasant views.

Solar energy is considered as one of the leading alternatives as life on earth relies on sun as it is fundamental energy source. Although mankind has been using solar energy extensively throughout history, solar energy has not been utilized for production of useful work directly until recently. Solar energy has been utilized for heating, electricity generation, lighting and some other minor purposes, such as desalination.

The available solar energy depends on time, geographical location and the economic feasibility of a solar system depends highly on available solar energy per collection area. Concentrating systems and solar tracking systems that follow direct sunlight are used to maximize solar flux. Although south of Turkey's annual average sum of global irradiation is about 2000 kWh/m^2 that is suitable for electricity generation, flat-plate collectors for domestic hot water systems are main solar energy utilization in Turkey and there is only negligible energy production. Germany 's annual average solar irradiation is half of that of Turkey's, but 3% of electricity consumed in Germany is generated by solar power.

One of the most important roadblocks for utilization of solar energy is its relatively high cost per power. Although fossil fuel costs are expected to increase due to limited resources, it is still expected to have a lower cost in the near future. Therefore, cost of energy produced from solar systems must be decreased so that it could become a competitive alternative. Reducing manufacturing costs and improving the performance of systems are required to reduce the cost per power for solar technologies and any means of improving the performance of the solar energy systems is critical.

There are two main approaches to produce useful work in the form of electricity using solar energy. The first one is by using photovoltaic systems, and the other is through solar thermal systems. While solar energy is directly converted to electricity by photovoltaic systems, it is transferred to a fluid using collectors and the heated fluid is used by a thermodynamic power cycle to generate electricity in solar thermal systems.

Solar photovoltaic (PV) systems comprised of arrays of cells containing semi conductor material that converts solar radiation into direct current (DC) electricity. Absorption of light, removes electrons from their atoms, and transfer them between bands generating an electron hole pair. This transfer results a voltage potential difference

between two electrodes. The photovoltaic effect (PV) was first observed by Becquerel in 1839 while working on a electrolytic cell that is made up from two metal electrodes. Research had been carried out in the past to identify different materials' photovoltaic conversion ability such as; selenium, copper, cuprous oxide, cadmium, germanium and silicone. While the efficiency of photovoltaic devices was 2% at 1950s, as a result of research carried out 14% efficiency achieved in 1960s. One of the major initial applications was a lighthouse with 242 W PV-array that is constructed in Japan in 1963. They have been used for space applications by NASA, and they have also been popularly used in mobile devices such as pocket calculators. More recently, they have been widely utilized in households by mounting on roof tops, and in electricity generation plants where large number of PV cells are combined into farms. The capacity of solar-PV farms of today range from 10-60 MW although proposed farms are on the order of 150 MW (Jacobson and Delucci, 2009).

Band gap of semiconductor shrinks and open circuit voltage decreases as temperature increases. Conversely, short current increases as the temperature increases because more charge carriers are moved from valance band to conduction band. Change in voltage dominates current with respect to changing temperature, power is product of voltage and current so efficiency of PV systems decreases with increasing operating temperature. Maximum theoretical efficiency of photovoltaic cells is defined by Shockley–Queisser limit and is around 33.7% at 1.1 eV (Shockley and Queisser, 1961). It is not actually possible to reach this efficiency due to major road blocks such as reflection from surface and blocking of incoming radiation due to thin cables on solar cell. Multiple layer solar cells have a theoretical limit of 86% and currently three junction concentration cells reached 43.5% efficiency (Kazmerski, 2005).

In solar thermal systems, solar energy is used to heat a working fluid (steam, synthetic oil or molten salt) for utilization in a thermodynamic power cycle. The maximum efficiency of a power cycle increases by increasing fluid temperature based on the second law of thermodynamics. Therefore, it is desired to heat the working fluid to high temperatures that can be achieved using concentrating systems. Incident solar energy over a large area is focused by an optical system that is usually comprised of reflectors or lenses to an absorber where the working fluid is heated in concentrating systems. The

heated working fluid is then used in a heat engine where a portion of the heat is converted to useful work in the form of electricity.

There are three common types of collectors that are used in solar thermal applications: Parabolic-trough reflectors as shown in Figure 1.3a focus light to heat a vacuum tube where working fluid flows. The mirrors surrounding the tower that are also known as heliostats focus light to the absorber located in the tower heating the working fluid in central tower receiver shown in Figure 1.3b. Lastly, parabolic dish receiver is shown in Figure 1.3c, which collect incoming radiation above the center of the dish.

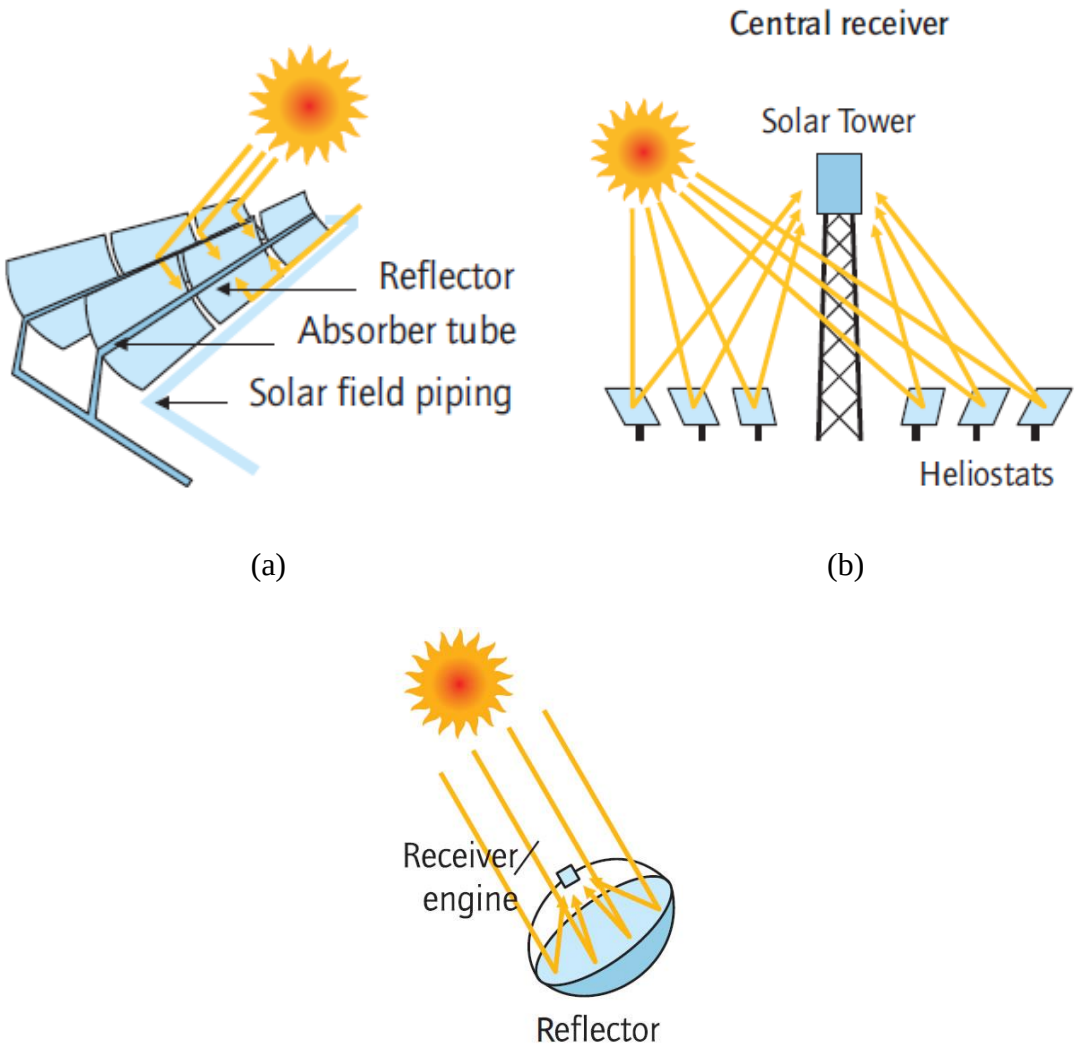

Figure 1.3. Concentrating collectors (a) Parabolic through collectors (b) Central tower receiver (c) Dish Systems (Philibert *et al.*, 2010).

These dishes have independent engines or PVs on its focal point, which eliminates use of working fluid.

A concentrating solar system comprises of three main sub-systems as shown in Figure 1.4. The first sub-system is the solar field where the solar energy is transferred to the working fluid. The second sub-system is the thermal storage unit where captured heat is stored in a high thermal capacity thermal storage media, such as pressurized steam, concrete, molten sodium nitrate, molten potassium nitrate or purified graphite, so that the concentrated solar power plant can also produce electricity at evenings where solar irradiation is not available. The third sub-section is the power block where useful work is produced by utilizing the working fluid with high availability in a turbine.

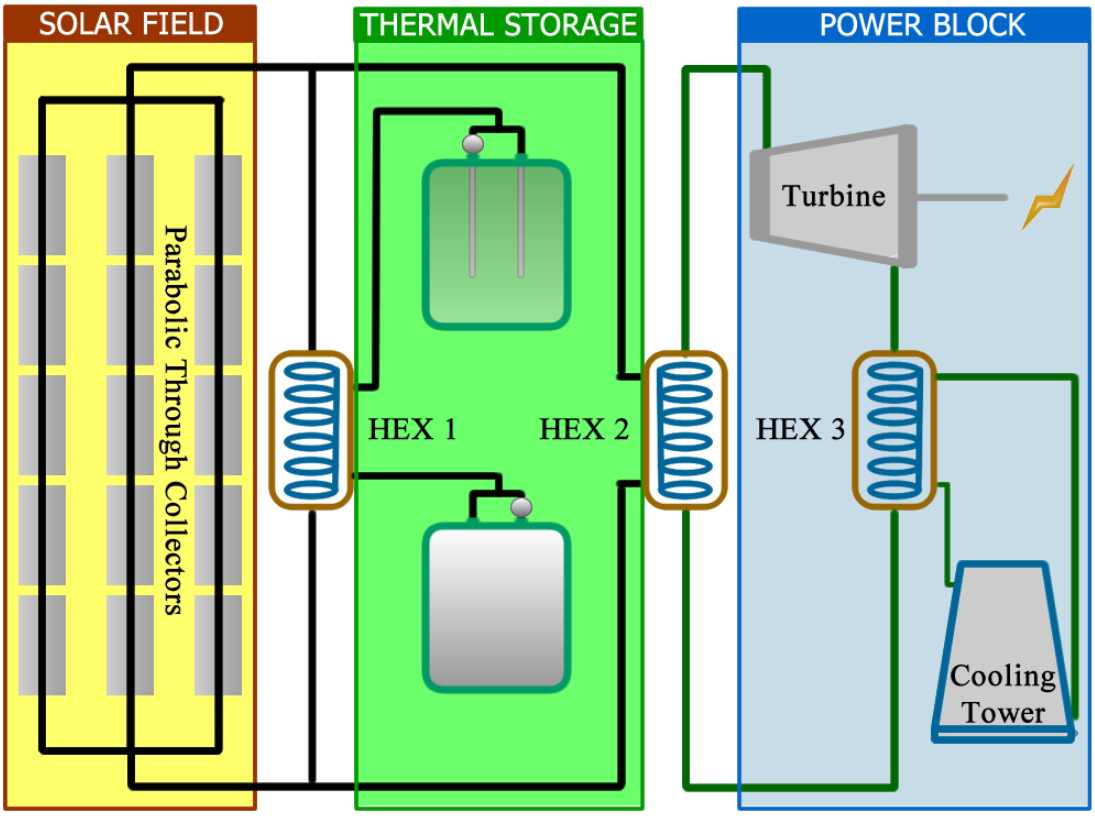

Figure 1.4. Overview of a concentrated solar power system.

Parabolic through systems are the most widely adopted concentrated solar power system. The absorber of a parabolic through system is usually comprised of a pipe that has an absorbing coating, surrounded by a transparent evacuated tube in order to minimize convective losses as shown in Figure 1.5. Radiative emission becomes the major heat loss mechanism in the absence of convective losses. Therefore, an ideal absorber must absorb as much solar energy as possible whereas it must emit as low heat as possible to environment.

Considering the high temperatures achieved in the absorbers due to concentration effect, the radiative heat lost can be significant, therefore special coatings should be used to maximize absorbed solar energy and minimize energy loss by emission of the absorber surface.

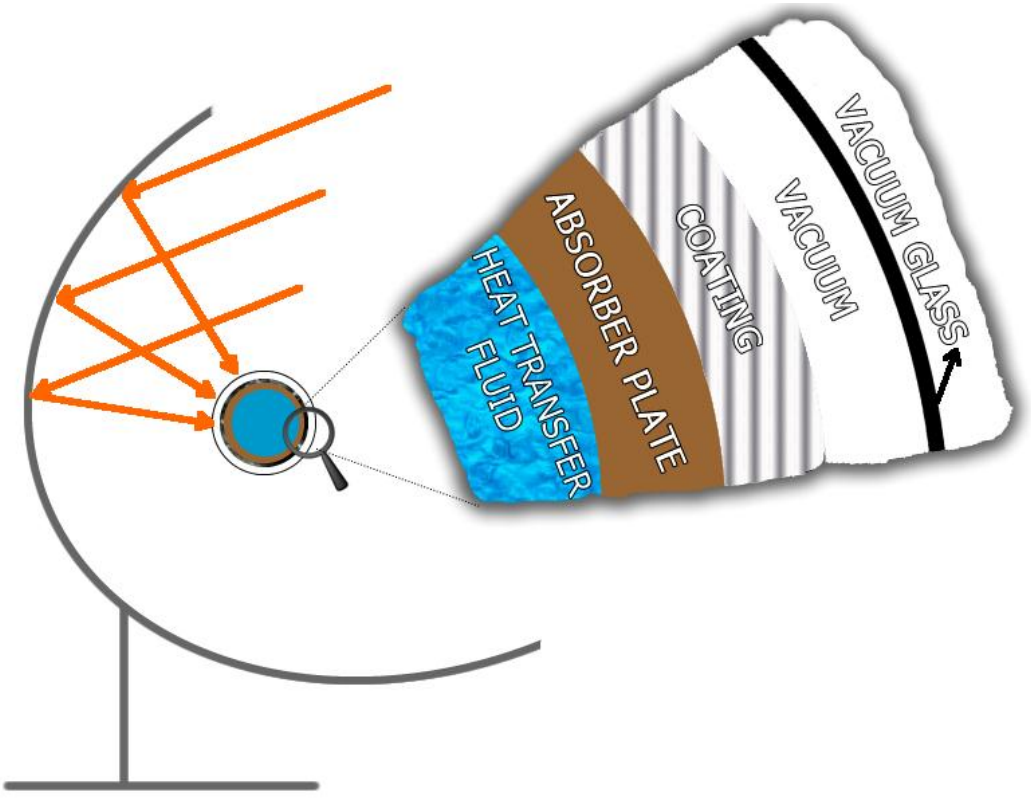

Figure 1.5. Cross section of absorber tube.

Solar radiation can be approximated as a blackbody heat source at 5777 K and is predominantly in the visible light wavelength range, 0.4-0.7 μm. Whereas, the radiation emitted by absorber is at infrared wavelengths, larger than 1μm, considering the typical absorber temperatures, as it is shown on Figure 1.6. Therefore, the ideal coating must have high absorptivity in shorter wavelengths, whereas it must have a high reflectivity in longer wavelengths.

In a solar system design, coatings have a very important role as they interact with incident radiation. As mentioned earlier, the ideal coating must be spectrally selective, absorbing at specific wavelengths and reflecting between specific wavelengths, as shown in Figure 1.6. In order to maximize the collection efficiency, coating must be designed based on the operating conditions of the system. Spectrally selective coatings can be categorized as (Kennedy, 2002):

(i) Intrinsic
(ii) Multilayer absorbers
(iii) Metal-dielectric composite coatings
(iv) Textured surfaces
(v) Semiconductor-metal tandems

Intrinsic materials have their own spectrally selective properties and used solitarily on substrate. They are stable but their efficiency is lower than multilayer absorbers. Metallic tungsten (W), silicon (Si) doped with boron (B), calcium fluoride (CaF_2), tin dioxide (SnO_2) are examples for intrinsic spectrally selective materials. Multilayer absorbers have high absorptance and low emittance and can be used at higher temperatures. Multiple reflections between layers increase absorptance. Different materials such as copper (Cu), silver (Ag), nickel (Ni) and dielectric layers such as silicon dioxide (SiO_2), zinc sulfide (ZnS), and aluminum oxide (Al_2O_3) can be used.

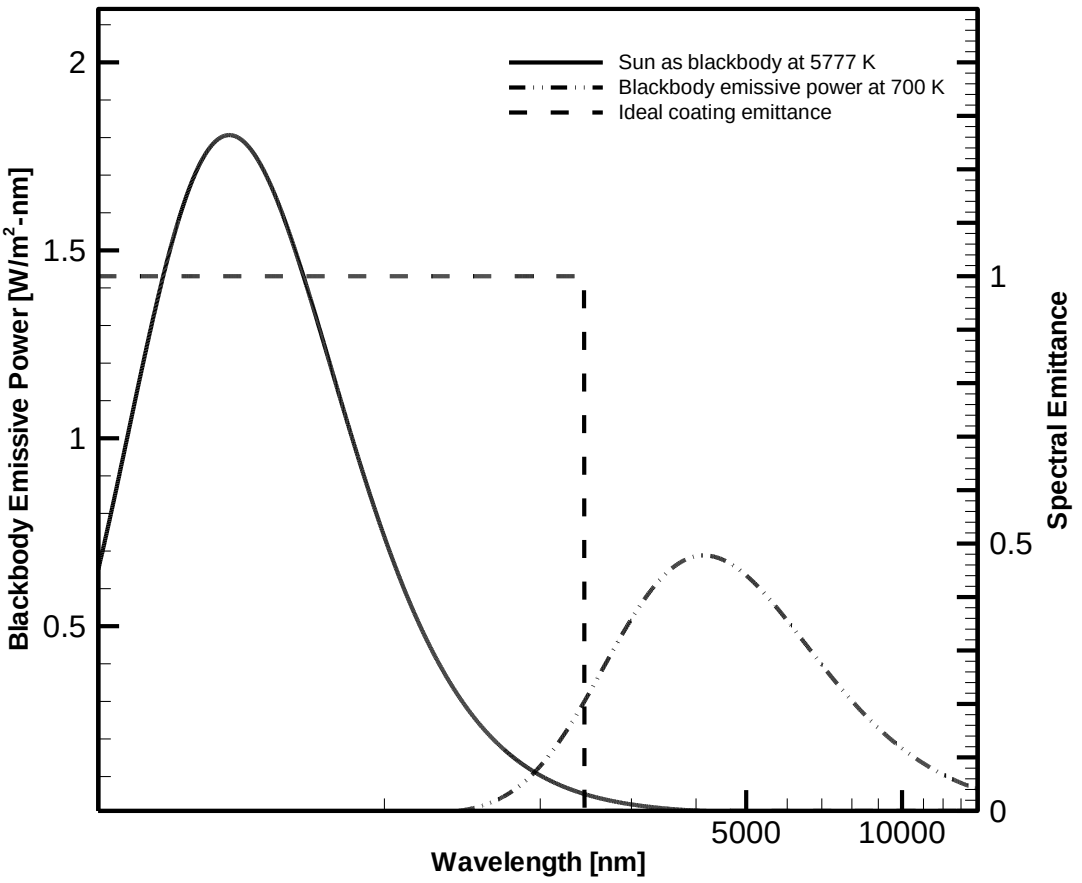

Figure 1.6. Distribution of solar irradiation and absorber emission, and ideal emissivity at various wavelengths.

Metal-dielectric composite or cermet coatings are highly absorptive in visible wavelengths and transparent at infrared. These composite contain fine metallic particles in a dielectric or ceramic matrix. Spectral selectivity can be optimized by changing volume fraction, coating thickness, particle size and shape. Oxidation of the metals is problem in this type of coating, for a stable radiative behavior, metals with low oxidation rates, can be used.

Dentritic and porous structures trap incoming radiation by multiple scattering in textured surfaces. Optical properties of a surface can be altered introducing such structures by ion-beam treatments, and spectrally selective behavior could be gained. Semiconductors, which has band gaps between 1 μm and 2.5 μm, such as lead sulfide

(PbS), germanium (Ge), and Si, have high absorptivity at short wavelengths. Anti-reflection coatings are necessary for such coatings as useful semiconductors have high refractive indices which cause reflective losses to be significant.

Pigmented coatings or paints are considered as metal-dielectric composite coatings and they consist of pigments and binder as shown in Figure 1.7. Their optical properties depend on pigment size, concentration, material, and resin material and thickness. Coatings with different optical properties can be produced by altering these properties. Carbon (C), PbS, Ni are mostly frequently used pigment materials used for solar absorbing coatings, whereas silicone or other polymers are used for resin material. Pigmented coatings most widely used coatings for low and mid temperature applications due to their low cost and ease of application. At higher temperatures (T >450 ^{o}C), polymer binder is not stable and additional process is required to stabilize the binder that increases its cost, and decreases its feasibility.

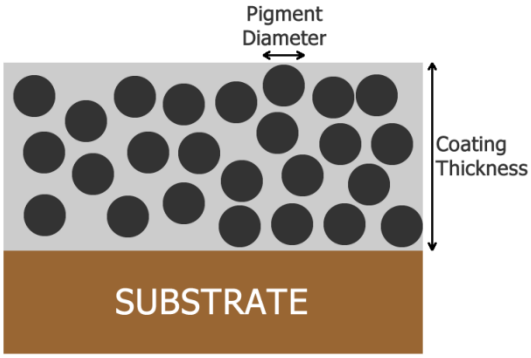

Figure 1.7. Pigmented coating.

1.2. Literature Survey

1.2.1. Overview and Earlier Studies

Solar thermal systems rely on transferring solar energy to a working fluid that is used in a thermodynamic cycle. Concentrating systems such as parabolic-through collectors are used to produce high temperature working fluids that are required for power cycles. Optical, thermal and thermodynamics analysis of collectors are studied extensively, and a

brief review of solar thermal systems and their applications are presented by Kalogirou (2003).

Most widely used solar coatings are pigmented coatings that comprise of a binder or a resin material and nano sized particles known as pigments embedded in the binder (Duffie and Beckman, 2006). The parameters affecting pigmented coating's radiative properties are optical properties of the pigment and resin materials, pigment size and concentration, and the thickness of the coating. Therefore, optimizing a spectrally selective pigmented coating for a particular application necessitates, estimation of these properties maximizing the performance of the solar system.

Radiative properties of solar coatings produced through different manufacturing processes were characterized experimentally in the earlier studies such as in Peterson and Ramsey (1975). Enhancing absorber's performance by using spectrally selective pigmented coatings is studied experimentally by Jurisson (1975). Coatings with cadmium telluride (CdTe) and PbS pigments are used and it is concluded that selective coatings can increase overall efficiency of solar energy collection systems significantly. Absorber's collection efficiency is dependent on pigment's size, volume fraction, resin thickness, and pigment and resin's optical properties as mentioned earlier. A summary of the earlier works on pigmented coatings are presented by Granqvist (1985) with comparisons of theoretical estimations based on effective medium theory and experimental results. However, considering the typical pigment sizes and concentrations, the use of effective medium theory is not applicable if the pigment size is not very small or in infrared wavelengths (Niklasson, 2006).

Experimental studies such as Jurrisson (1975) consider only limited number of combinations of these parameters and in order to find the optimal parameters for the ideal coating a mathematical model must be developed. After constructing a detailed model, suitable coating properties could be estimated easily.

1.2.2. Modeling of Pigmented Coatings

The radiative behavior of pigments in a binder must be modeled in order to construct a model for pigmented coatings. Modeling radiative behavior of pigments in a binder is analogous to modeling radiative behavior of a cloud of spherical particles in a dielectric medium. Radiative properties of a sphere cloud can be predicted by solving Maxwell equations representing the electromagnetic field. However, solving Maxwell equations for a particle cloud is computationally expensive. An approximation of the problem could be considered for a simpler solution even though some limitations exist. In 1908 Gustav Mie developed an analytical solution to Maxwell equations, considering independent scattering around a single spherical particle, neglecting the effects of any neighboring particle (Mie, 1908). Incident plane wave and scattering field is expanded into radiating spherical vector wave functions in Mie's solution, also known as Lorenz-Mie theory.

Mie solution is the simplest approach to represent electromagnetic scattering of particles when particle size is in the order of wavelength of radiation. Although there are simpler approaches such as Rayleigh scattering, which can describe scattering by particles that are much smaller than the wavelength of radiation, Rayleigh scattering is not valid for pigment clouds as pigment size is close to wavelength of incident wave. In dense mediums and very high and very low size parameters, where size parameter describes the size of the particle relative to the wavelength of radiation, the effects of the neighboring particles are no more negligible. In such a case, dependent scattering must be considered, where effects of neighboring particles are taken in to consideration, along with multiple scattering effects. Brewster and Tien (1982) and Hottel *et al.* (1970) reported different criteria for describing the scattering regime and a standard regime map is presented in Figure 1.8.

Once the radiative behavior of pigments are identified using Mie solution considering independent scattering, the radiative behavior of pigmented coatings can be estimated based on Kubelka-Munk theory. Kubelka-Munk theory is based on two-flux model that describe radiative behavior of thin translucent films subject to diffuse irradiation. Extended Kubelka-Munk theory was developed by Vargas and Niklasson (1997c) to consider collimated radiation rather than diffuse. Use of extended Kubelka-Munk theory is

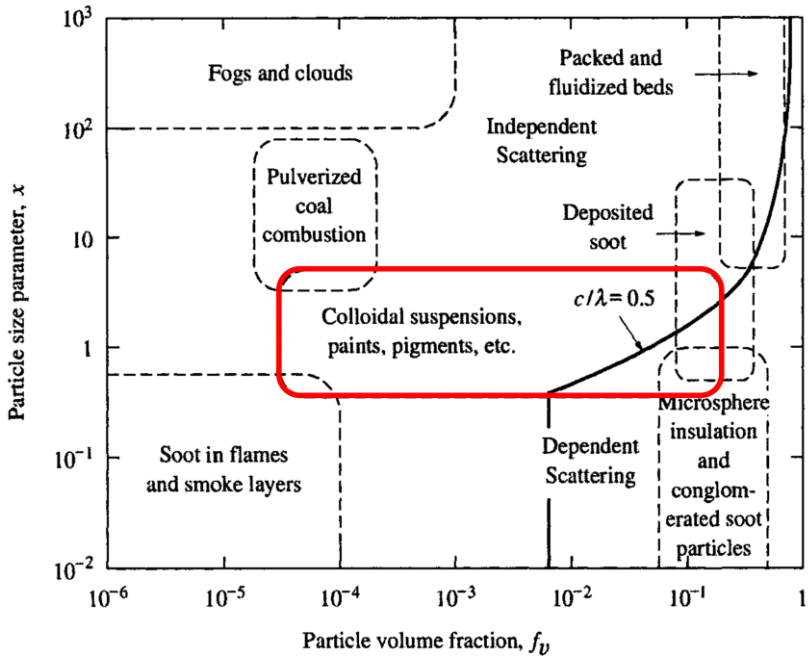

Figure 1.8. Scattering regime map (Siegel and Howell, 1992).

more appropriate for solar coatings as they are subject to collimated irradiation rather than diffuse.

Effects of multiple scattering can be incorporated in such a formulation by the use of Hartel theory as presented by Vargas and Niklasson (1997d) for calculating average pathlength parameters and forward scattering ratios. Hartel theory is not capable of handling optically thick films that contains non-absorbing particles (Vargas and Niklasson, 1997b). In case of radiative cooling applications where the goal is reflecting at near infrared and infrared wavelengths, non-absorbing particles at a low volume fraction are used as pigments and extended Hartel theory is used considering the average pathlength parameters corresponding to the different scattering orders (Vargas and Niklasson, 1997b).

The accuracy of the Kubelka-Munk theory can be improved by using four-flux method developed by Maheu *et al.* (1997) that considers both collimated and diffuse components of radiation in conjunction with Lorenz-Mie and extended Hartel theories (Vargas, 1998). The developed model based on four-flux method in conjunction with

Lorenz-Mie and Hartel theory is validated by experimental measurements, for a reflective coating with rutile titanium dioxide (TiO_2) pigments in silicone resin (Vargas *et al.*, 2000).

When particles or pigments are spaced closely with respect to the wavelength, the light scattered by a single particle is no more independent of its neighboring particles that is known as dependent scattering (Howell *et al.*, 2011). Maxwell equations must be solved for multiple particles in this case that can be computationally demanding. There are various methods of solution for dependent scattering such as transition matrix (T-matrix) method, discrete dipole approximation (DDA) and finite element method (FEM). Discrete dipole approximation is a powerful method and it is generally used for agglomerates that are not spherical and have much larger area-volume ratio (Howell *et al.*, 2011). Finite element method can handle various problems such as different shapes and inhomogeneous medium and commercial software such as COMSOL rely on FEM for solving Maxwell equations. T-matrix method handles dependent scattering as an extension of Mie scattering. Optical properties and scattering behavior of spheres in cluster are calculated individually and also cluster is considered as a whole thus scattering and absorption coefficients of the cluster are calculated accordingly (Vargas, 2003) in T-matrix method.

Vargas (2003) considered the effects of dependent scattering on pigmented coatings by using T-matrix method to estimate the absorption and scattering cross sections of the randomly oriented particle clusters instead of the Lorenz-Mie theory, whereas four flux method is used to estimate the reflectance of the coating. Differences in cross-sections, forward scattering ratio, forward average crossing parameter, total absorption and reflection are presented, and it was observed that models based on dependent and independent scattering results in similar predictions of reflectance for the visible light, whereas deviation is observed for near infrared wavelengths.

When particle size is too small with respect to wavelength, neither Mie solution, nor T-matrix method cannot be applied. Effective Medium Theory (EMT) must be used to find scattering and absorption efficiencies in small particles. Most popular EMT approximations are Maxwell-Garnett and Bruggeman theory that are presented in detail by Niklasson (1981).

1.2.3. Optimization and Parametric Studies

Following the studies outlining the theoretical framework for modeling of pigmented coatings optimization studies have been performed. Effects of particle size and volume fraction are presented by Vargas (2000) through a parametric study. The solar coatings investigated by Vargas *et al.* (1998, 2000), Vargas and Niklasson (2001) and Vargas (2000). are coatings with TiO_2 or SiO_2 pigments mostly used to achieve light colored coatings for radiative cooling applications.

Theoretical investigation of thickness sensitive, spectrally selective solar absorber coatings are investigated by Etherden *et al.* (2004). They used Lorenz-Mie theory to estimate the single scattering absorption and scattering cross sections and four flux method to estimate the spectral emittance. A parametric study was carried out predicting the solar absorptance that is to be maximized and total emittance that is to be minimized.

A similar optimization study is carried out by Zhao and Wackelgard (2006) for spectrally selective three-layer coatings. In this study the coating is modeled based on EMT and volume fraction and thickness are optimized. The pigment radius was not estimated as it does not appear in the EMT model based on Maxwell-Garnett theory. They have also carried out an experimental study to validate their model.

More recently, Baneshi *et al.* (2009) used Lorenz-Mie theory and radiation element method by ray emission model (REM^2) for optimizing TiO_2 based coatings for thermal and aesthetic effects where radiative cooling is desired while minimizing the glare for buildings. An optimization parameter defined based on the ratio of reflectance in near infrared wavelengths to reflectance in visible range, optimal pigment size, volume fraction and coating thickness is estimated through a parametric study. Baneshi *et al.* (2011) presented a comparison of CuO and TiO_2 pigmented coatings for radiative cooling using a similar approach.

1.3. Objective of Study

The pigmented coating design problem can be considered as predicting the pigment size, pigment volume fraction that yields or best approximates the ideal coating's spectral emittance. Although a size range was presented for optimal radius of various pigments in studies such as Etherden *et al.* (2004), an optimal design have not been presented. This study aims at presenting a design methodology for optimization of spectrally selective pigmented coating for solar thermal systems.

In order to achieve this goal, a unified model of the pigmented coating, considering different scattering regimes including EMT, independent and dependent scattering, where four flux method is used for solution of radiative transfer equation, is developed for the first time. The unified models will be developed combining formulations presented by Vargas and Niklasson (1997c,d), Maheu *et al.* (1984), and Vargas (1998).

Once a unified model of the spectrally selective coating is developed and validated, the design problem can be considered. An ideal spectral emittance for the coating can be defined based on system's operating conditions and the goal of such a design problem is to estimate the design variables, such as pigment size, concentration, material, resin material and thickness, to achieve the ideal coating behavior. Such a design problem can be considered as an inverse problem where the system exhibiting a desired behavior under known conditions is to be identified. Considering the non-linear nature of the problem, the inverse design problem will be solved by non-linear optimization methods as explained in Howell *et al.* (2003) and Daun *et al.* (2002).

2. RADIATIVE TRANSFER MODEL OF PIGMENTED COATINGS

The pigmented coating applied on a metallic substrate can be considered as a thin slab as shown in Figure 2.1 that is illuminated from one side. The radiative behavior of the coating with respect to an incident electromagnetic wave can then be determined by solving the Maxwell equations for the system as shown below. The solution of Maxwell equations considering all the details of the complete system is computationally very demanding and is not feasible. However, the modeling of the system is possible through the solution of radiative transfer equation (RTE) considering radiative transport behavior of each layer represented in the form of absorption, scattering coefficients, and scattering phase function.

The pigmented coating in the system presented is absorbing, emitting and anisotropically scattering medium and an analytical solution of the RTE for such as system is not possible, and a numerical solution procedure must be adopted. The problem can be considered in terms of two sub-problems:

(i) Prediction of radiative properties of the pigmented coating
(ii) Solution of RTE based on the predicted radiative properties

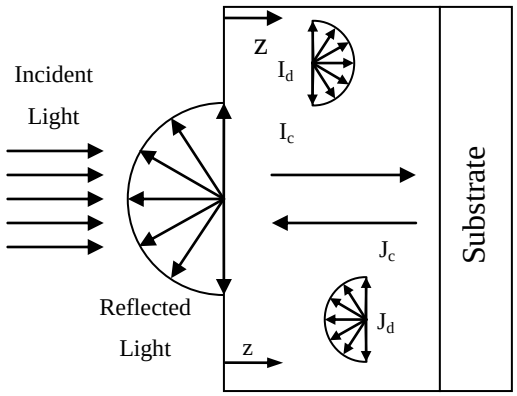

Figure 2.1. Sketch of the spectrally selective coating on a substrate.

2.1. Prediction of Radiative Properties

When electromagnetic waves interact with particles some of their energy is absorbed while the rest is scattered. The amount of scattered and absorbed energy can be represented in terms of radiative transport properties such as absorption and scattering coefficients where these can be estimated by direct solution of Maxwell equations. Models relying on approximate solutions can be used to predict the radiative properties since a direct solution requires significant computation effort. These approximate models are valid under certain scattering regimes; therefore, it is important to understand the scattering regime and use the correct approximate model.

Size of the pigment with respect to incoming radiation wavelength plays an important role on identifying the scattering regime and the relative effect can be identified in terms of a size parameter, which represents the ratio of pigment size to wavelength, given by Equation 2.1. Moreover, effect of neighboring particles becomes significant when pigments in the binder are closer. Therefore, particle size parameter and volume fraction can be used to identify the scattering regime.

$$x = \frac{2\pi m_2 r_p}{\lambda} \tag{2.1}$$

Howell *et al.* (2011) have presented a scattering regime map that describes the scattering behavior in terms of particle size parameter and particle volume fraction as shown in Figure 2.2. If the clearance between neighboring particles are relatively larger ($c/\lambda > 0.3$) scattering due to a particle is not effected by neighboring particles and this is known as independent scattering. If clearance ratio is smaller than 0.3 then the scattering is affected by the existence of neighboring particles and scattering is considered as dependent. If the size parameter is smaller than 0.2 then particles in medium behave as a continuous, homogenous medium, and effective medium theory is used to find optical properties (Niklasson, 2006).

For solving single independent scattering, Lorenz-Mie theory can be used and it is valid at $0.3 < x < 5$ (Mie, 1908). When distance between particles get smaller and volume

fraction increases, probability of scattered beam of a particle to scatter from other particles increases. This physical phenomena effects optical property of particle cluster. Hartel (1940) calculated the effect of multiple scattering, therefore, Lorenz-Mie theory in conjunction with Hartel theory is used to calculate independent multiple scattering. Single independent scattering is not used solitarily in this study as volume fraction for absorbing coatings is larger than 0.02, which is out of single independent scattering region as presented in Figure 2.2.

T-Matrix method that is considered as an extension of Lorenz-Mie theory for solving dependent scattering. can be used to model dependent scattering. Although T-Matrix method can also be used to model independent scattering as well, independent scattering is

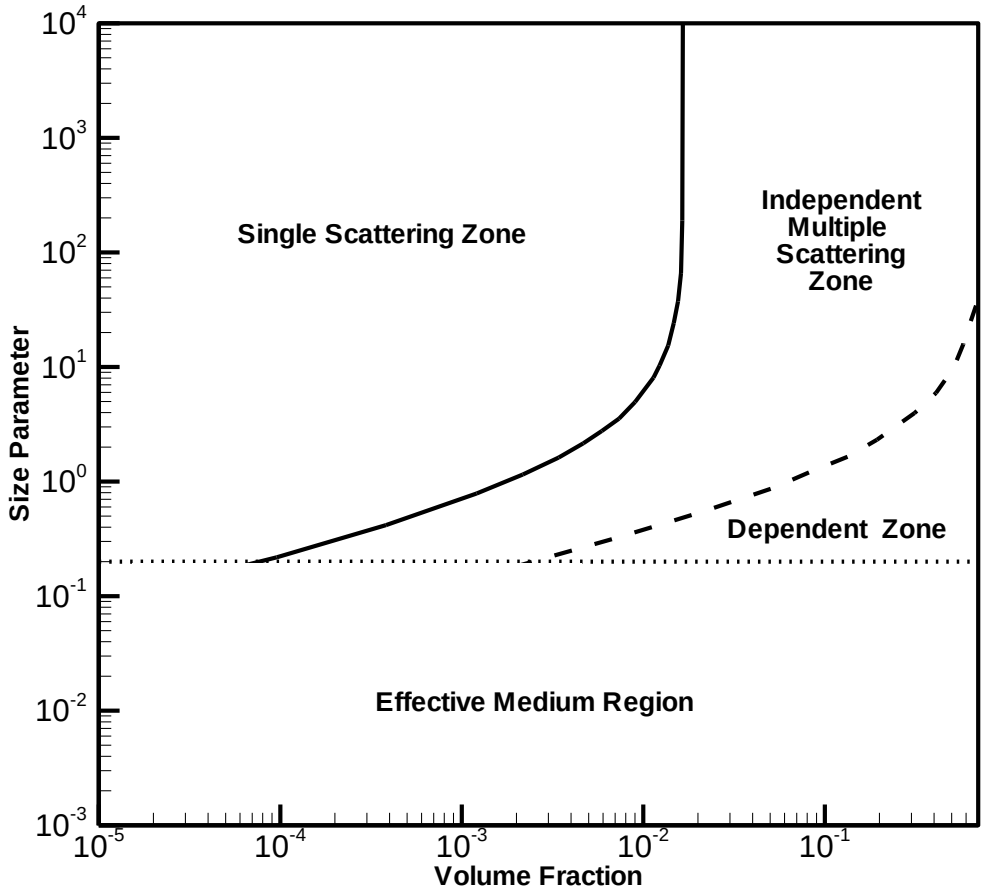

Figure 2.2. Effective medium, single and multiple (dependent and independent) scattering regimes.

not handled by T-Matrix method as the computational effort required by T-Matrix method is significantly higher than Lorenz-Mie theory in conjunction with Hartel theory.

Lorenz-Mie theory is not valid for scattering problems with small size parameters as mentioned earlier. Particles and the medium behave as a unified continuous and homogenous medium for size parameters smaller than 0.2, and effective medium theory is used to find optical properties of this medium (Niklasson, 2006).

2.1.1. Effective Medium Theory

When particle size is very small with respect to wavelength, pigments and matrix behave as a single homogenous medium. Lorenz-Mie theory is not valid for scattering problems of small pigments as mentioned earlier. Therefore, in order to find optical properties of such small particles in a matrix, effective medium theory (EMT) can be used. There are various effective medium theories and Maxwell-Garnett and the Bruggeman theories are the widest used theories (Bohren, 1986). Bruggeman theory is used for aggregated structure where distinction is not possible whereas Maxwell-Garnett is used for distinguishable, separated grain structures like pigmented coatings. Therefore Maxwell-Garnett theory is used in this study. Pigmented coating is considered as homogeneous material from macroscopic point of view and the optical properties are represented in terms on effective properties in EMT.

The reflectivity of an absorbing thin film coating on a metal substrate can be estimated based on net radiation method by

$$R_\lambda = \frac{\rho_1 + \rho_2(1-2\rho_1)\exp(-2a_1L)}{1-\rho_1\rho_2\exp(-2a_1L)} \tag{2.2}$$

where $a_1 = 4\pi k_1/\lambda$, spectral reflectivity at air to coating boundary is

$$\rho_1 = \frac{(n_1-1)^2 + k_1^{\,2}}{(n_1+1)^2 + k_1^{\,2}} \tag{2.3}$$

and spectral reflectivity at coating to substrate boundary is

$$\rho_2 = \frac{(n_2 - n_1)^2 + (k_2 - k_1)^2}{(n_2 + n_1)^2 + (k_2 + k_1)^2} \tag{2.4}$$

The refractive indices in Equation 2.2-4 can be represented in terms of dielectric permeability as:

$$n^2 = \frac{1}{2}\left(\varepsilon' + \sqrt{\varepsilon'^2 + \varepsilon''^2}\right)$$

$$k^2 = \frac{1}{2}\left(-\varepsilon' + \sqrt{\varepsilon'^2 + \varepsilon''^2}\right)$$

where $\varepsilon = \varepsilon' - i\varepsilon''$, $\varepsilon' = n^2 - k^2$, and $\varepsilon'' = 2nk$.

The effective dielectric permeability of pigmented coating can then be estimated using Maxwell-Garnett theory as a function of dielectric permeability of pigment, matrix and particle volume fraction that is represented as:

$$\bar{\varepsilon}_\lambda^{MG} = \varepsilon_r \frac{\varepsilon_p + 2\varepsilon_r + 2f_v(\varepsilon_p - \varepsilon_r)}{\varepsilon_p + 2\varepsilon_r - f_v(\varepsilon_p - \varepsilon_r)} \tag{2.5}$$

Effective medium theory considers a homogenous medium so that pigmented coating and scattering from particles does not exist in the model anymore.

2.1.2. Lorenz-Mie Theory

Lorenz-Mie theory is used to define scattering and absorption behavior of a single scattering medium consisting of spherical particles that relies on solution of Maxwell equations (Howell *et al.*, 2011). Therefore, Lorenz-Mie theory can be used to model the radiative behavior of the pigmented coating approximating pigments as uniformly sized spheres and considering the matrix material as dielectric. The former of these

approximations is a quite reasonable considering the characterization presented by Vargas and Niklasson (1997a), whereas the latter one can be justified considering the extinction index, imaginary part of complex refraction index, of polymeric binders that are smaller than 0.003 throughout the entire spectrum.

The Lorenz-Mie theory neglects the effects of neighboring particles that is valid if clearance to wavelength ratio is larger than 0.3 (Brewster and Tien, 1982). Although at longer wavelengths and denser particle volume concentrations dependent scattering regime will prevail, independent scattering approximation still yields reasonable accuracy (Vargas, 2003).

Mie coefficients a_n and b_n are expressed in terms of Ricatti-Bessel functions, ψ_n and ξ_n as

$$a_n = \frac{m\psi_n(mx)\psi_n'(x) - \psi_n(x)\psi_n'(mx)}{m\psi_n(mx)\xi_n'(x) - \xi_n(x)\psi_n'(mx)}$$

$$b_n = \frac{\psi_n(mx)\psi_n'(x) - m\psi_n(x)\psi_n'(mx)}{\psi_n(mx)\xi_n'(x) - m\xi_n(x)\psi_n'(mx)}$$

Here the relative refractive index, m is

$$m = \frac{n_1 + k_1 \cdot i}{n_2}$$

where n_1, k_1 are the refractive and extinction index for the pigment material, and n_2 is the refractive index for the matrix. The scattering, extinction and absorption cross sections, $C_{sca,\lambda}$, $C_{ext,\lambda}$ and $C_{abs,\lambda}$ are defined as where summation from 1 up to $x + 4 \cdot x^{1/3} + 2$ gives adequate accuracy.

$$C_{ext,\lambda} = \frac{2\pi {r_p}^2}{x^2} \sum_{n=1}^{\infty} (2n+1)\,\mathrm{Re}(a_n + b_n) \tag{2.6}$$

$$C_{sca,\lambda} = \frac{2\pi {r_p}^2}{x^2} \sum_{n=1}^{\infty} (2n+1)(|a_n|^2 + |b_n|^2) \tag{2.7}$$

$$C_{abs,\lambda} = C_{ext,\lambda} - C_{sca,\lambda} \tag{2.8}$$

Pigmented coatings are usually very thin, however due to high particle volume concentration, multiple scattering occur that is not captured by Lorenz-Mie theory. Therefore, Hartel theory is used in order to consider multiple scattering effects. Hartel theory works well with thin coatings as suggested in (Hottel *et al.*, 1970). However, if the coating is thick and particles are non-absorbing, Hartel's theory shows an anomalous behavior (Vargas and Niklasson, 1997b), and extended Hartel theory must be used for those cases. Hartel theory is used in this study as pigmented coatings for solar applications has thin matrix and absorbing particles. The formulation of the Hartel theory is adopted in this study from Vargas and Niklasson (1997b) and presented in Appendix A

2.1.3. T-Matrix Method

When clearance to wavelength ratio gets smaller, effect of neighboring particles become significant. This effect arises from two reasons: First, radiation scattered from a particle can interfere with scattered radiation from another particle that is called far field effect. Second, the internal radiation field of a particle can be effected by scattering by neighboring particles that is called the near field effect. T-matrix method, also known as Extended Boundary Condition Method (EBCM) or Null-Field Method (NFM), is a general solution method to electromagnetic field equations that is applicable to dependent or independent scattering problems of spherical or non-spherical particles. The formulation is considered as an extension of Lorenz-Mie theory for multiple particles. Scattering field only consists of scattering due to single particle in Lorenz-Mie theory, whereas it is predicted considering the effect of all particles in the T-matrix method.

Incident and scattering fields are expended by regular and outgoing vector spherical wave function (VSWF) expansions, respectively. When continuity equations at the surface

of every spheroid are applied, the result is a system of interaction equations for the scattered field coefficients. The solution of scattered field can be presented as

$$a_{mnp}^{i} - \bar{a}_{np}^{i} \sum_{\substack{j=1 \\ j\neq i}}^{N_s} \sum_{l=1}^{L_i} \sum_{k=-l}^{l} \sum_{q=1}^{2} H_{mnpklq}^{i-j} a_{klq}^{j} = \bar{a}_{np}^{i} f_{mnp}^{i} \tag{2.9}$$

In order to solve a set of Equation 2.9, iterative methods are used as recursive algorithms are numerically unstable.

Coefficients for incident field vector spherical wave function expansion for a plane wave that centered about origin are

$$\begin{pmatrix} f_{mnp,\hat{\beta},PW} \\ f_{mnp,\alpha,PW} \end{pmatrix} = -4\pi i^{n+1} e^{-im\alpha} \begin{pmatrix} \tau_{mnp}(\cos\beta) \\ i\,\tau_{mn(3-p)}(\cos\beta) \end{pmatrix}$$

Where τ_{mnp} is calculated from vector spherical harmonic functions

$$\tau_{mnp}(\cos\beta) = \frac{(-1)^m}{2} \left(\frac{1}{4\pi(2n+1)} \right)^{1/2} \left((-1)^p D_{m1}^{(n)}(\cos\beta) \right) + D_{m1}^{(n)}(\cos\beta)$$

Scattering properties are independent of direction of light incident on a sphere when considering a single spherical particle. However, for a particle cluster, scattering properties depend on direction of incident radiation with respect to cluster arrangement. Random option is selected in order to consider any arbitrary direction in the calculations and calculate orientation averaged scattering properties.

Codes for T-matrix method is adopted from Mackowski and Mishchenko (2011) and used to handle dependent scattering.

2.2. Solution of Radiative Transfer Equation for Pigmented Coatings

The pigmented coating applied on a metal substrate can be considered as a thin slab as shown in Figure 2.1 that is illuminated from one side. There are different methods that can be used for solution of radiative transfer equation for the one dimensional thin slab problems shown in Figure 2.1. Kubelka-Munk theory that is a two flux approximation and four flux method are most widely used methods (Vargas and Niklasson, 1997c,d; Maheu *et al.*, 1984; Vargas, 1998).

Under collimated beam using four flux method is more appropriate as Kubelka-Munk theory considers only diffuse illumination. The four flux method considers four intensities as shown in Figure 2.1 (I_d, diffuse forward; J_d, diffuse backward; I_c, collimated forward; J_c, collimated backward) traveling through the slab. This yields four coupled linear differential equations for each intensity component that can be presented as:

$$\frac{dI_{c,\lambda}}{dz} = -(\sigma_{s,\lambda} + \beta_\lambda) I_{c,\lambda} \tag{2.10}$$

$$\frac{dJ_{c,\lambda}}{dz} = (\sigma_{s,\lambda} + \beta_\lambda) J_{c,\lambda} \tag{2.11}$$

$$\begin{aligned} \frac{dI_{d,\lambda}}{dz} = &-\xi\beta_\lambda I_{d,\lambda} - \xi(1-\sigma_d)\sigma_{s,\lambda} I_{d,\lambda} + \\ &\xi(1-\sigma_d)\sigma_{s,\lambda} J_{d,\lambda} + \sigma_c \sigma_{s,\lambda} I_{c,\lambda} + (1-\sigma_c)\sigma_{s,\lambda} I_{c,\lambda} \end{aligned} \tag{2.12}$$

$$\begin{aligned} \frac{dJ_{d,\lambda}}{dz} = &\xi\beta_\lambda I_{d,\lambda} + \xi(1-\sigma_d)\sigma_{s,\lambda} J_{d,\lambda} - \\ &\xi(1-\sigma_d)\sigma_{s,\lambda} I_{d,\lambda} - \sigma_c \sigma_{s,\lambda} J_{c,\lambda} - (1-\sigma_c)\sigma_{s,\lambda} I_{c,\lambda} \end{aligned} \tag{2.13}$$

The spectral scattering and extinction coefficients $\sigma_{s,\lambda}$ and β_λ, are calculated by scattering models from:

$$\sigma_{s,\lambda} = \frac{f_v \cdot C_{sca,\lambda}}{V} \tag{2.14}$$

$$\beta_\lambda = \frac{f_v \cdot C_{ext,\lambda}}{V} \tag{2.15}$$

For independent scattering, most of the parameters used in four flux method are predicted by Lorenz-Mie theory. However, as the theory considers single scattering approximation and the problem considered is prone to multiple scattering, diffuse forward scattering ratio and average pathlength parameter cannot be predicted. Here, same forward scattering values for diffuse and collimated radiation can be considered following the analysis in Etherden *et al.* (2004) assuming an average pathlength parameter, ξ=2. However, a more correct prediction of these parameters is possible by using Hartel theory as presented in Vargas and Niklasson (1997b).

The forward scattering ratio, σ_c, defines the ratio of forward scattering to all scattering for the collimated beam and represented as

$$\sigma_c = \frac{\int_0^1 p(\mu) \cdot d\mu}{\int_{-1}^1 p(\mu) \cdot d\mu} \tag{2.16}$$

where $p(\mu)$ is the scattering phase function, μ=cos(θ), θ being the polar angle. The phase function can be represented in terms of Legendre polynomials and evaluating Equation 2.16 is possible with numerical integration. However, numerical integration using Legendre polynomials is computationally expensive and integrated form of forward scattering ratio is used in this study which was described in detail and presented in Vargas and Niklasson (1997b). The integrated form of forward scattering ratio is presented

$$\sigma_c = \frac{1}{2} - \left(\frac{2}{\delta}\right) \sum_{m=2}^{\infty} \sum_{n=1}^{\infty} p_{nm} \, \mathrm{Re}\left(a_m a_n^{\,*} + b_m b_n^{\,*}\right) - \left(\frac{2}{\delta}\right) \sum_{m=1}^{\infty} \sum_{n=1}^{\infty} q_{nm} \, \mathrm{Re}\left(a_m b_n^{\,*}\right) \tag{2.17}$$

where

$$\delta = x^2 Q_{sca,\lambda}$$

$$p_{nm} = (-1)^{(m+n-1)/2} \frac{(2m+1)(2n+1)(m-1)!!\,n!!}{(m-n)(m+n+1)m!!\,(n-1)!!}$$

$$q_{nm} = (-1)^{(m+n)/2} \frac{(2m+1)(2n+1)m!!\,n!!}{m(m+1)n(n+1)(m-1)!!\,(n-1)!!}$$

Scattering phase function could be written in terms of Legendre polynomials as mentioned before. One can observe angular distribution of scattered light from a particle from phase function. Details of formulation for multiple scattering are given in Appendix A.

Hartel theory behaves anomalously at optically thick films containing non absorbing particles where extended Hartel theory must be used. As this study contains absorbing particles, Hartel theory yields accurate results. Therefore, Hartel theory is used to estimate average pathlength parameter and diffuse forward scattering ratio. It should be noted that the value of average pathlength parameter is observed to be approximately 2, as suggested in Etherden *et al.* (2004).

Diffuse forward scattering ratio is assumed to be equal to the collimated one in four flux model presented in Maheu *et al.* (1984). The collimated and diffuse forward scattering ratios and formulation presented in Vargas and Niklasson (1997b) is adopted for prediction of diffuse forward scattering ratio.

Spectral reflectance is defined as ratio of reflected spectral intensity to incident spectral intensity and it can be estimated by solution of Equation 2.10-13. Following Equation 2.10-13, spectral reflectance has two components; diffuse and collimated, that can be expressed as:

$$R_{c,\lambda} = r_c + \frac{(1-r_c)^2 r_c' \exp(-2(\sigma_{s,\lambda} + \beta_\lambda)t)}{1 - r_c r_c' \exp(-2(\sigma_{s,\lambda} + \beta_\lambda)t)} \tag{2.18}$$

$$R_{d,\lambda} = \frac{\left\{\begin{array}{l}\left[(1-r_d)(1-r_c)\exp(-(\sigma_{s,\lambda}+\beta_\lambda)t)\right]\times \\ \left[C_0 + C_1\exp((\sigma_{s,\lambda}+\beta_\lambda)t) + C_2\exp(-(\sigma_{s,\lambda}+\beta_\lambda)t)\right]\end{array}\right\}}{\left\{\begin{array}{l}\left[\begin{array}{l}(A_1^2-(\sigma_{s,\lambda}+\beta_\lambda)^2)\times \\ (1-r_c r_c'\exp(-2(\sigma_{s,\lambda}+\beta_\lambda)t))\end{array}\right]\times \\ \left[A_1(r_d r_d'-1)\right]\cosh(A_1 t) + \left[A_5(r_d'+r_d) - A_4(1+r_d r_d')\sinh(A_1 t)\right]\end{array}\right\}} \qquad (2.19)$$

Equation 2.19 is presented in terms of variables C_0, C_1, C_2 and A_1,..,A_5 that are defined as:

$$C_0 = A_1\left[(A_3 + r_c' A_2) - r_d'(A_2 + r_c' A_3)\right]$$

$$C_1 = \left[A_1(r_d' A_2 - A_3)\right]\cosh(A_1 t) + \left[A_2(A_5 - r_d' A_4) + A_3(r_d' A_5 - A_4)\right]\sinh(A_1 t)$$

$$C_2 = r_c'\left\{\left[A_1(r_d' A_3 - A_2)\right]\cosh(A_1 t) + \left[A_3(A_5 - r_d' A_4) + A_2(r_d' A_5 - A_4)\right]\sinh(A_1 t)\right\}$$

$$A_1 = \xi\sqrt{\beta_\lambda[\beta_\lambda + 2\sigma_{s,\lambda}(1-\sigma_d)]}$$

$$A_2 = \sigma_{s,\lambda}[\xi\beta_\lambda\sigma_c + \xi\sigma_{s,\lambda}(1-\sigma_d) + (\sigma_{s,\lambda}+\beta_\lambda)\sigma_c]$$

$$A_3 = \sigma_{s,\lambda}\{\xi[\sigma_{s,\lambda}(1-\sigma_d) + \beta_\lambda(1-\sigma_c) - (\sigma_{s,\lambda}+\beta_\lambda)(1-\sigma_c)]\}$$

$$A_4 = \xi[\sigma_{s,\lambda} + \beta_\lambda(1-\sigma_d)]$$

$$A_5 = \xi\sigma_{s,\lambda}(1-\sigma_d)$$

The collimated and diffuse components of spectral reflectance also depends on reflectivities at the boundaries as shown in Equation 2.18 and Equation 2.19. The parallel and perpendicular components of the reflected electric field is given as

$$E_{//} = \frac{\cos\theta/\cos\chi - (n_1 - ik_1)/(n_2 - ik_2)}{\cos\theta/\cos\chi + (n_1 - ik_1)/(n_2 - ik_2)}$$

$$E_{\perp} = -\frac{\cos\chi/\cos\theta - (n_1 - ik_1)/(n_2 - ik_2)}{\cos\chi/\cos\theta + (n_1 - ik_1)/(n_2 - ik_2)}$$

By using Snell's law, the angle of refraction, χ, can be written in terms of angle of incidence, θ, and refractive indices as:

$$\frac{\sin\chi}{\sin\theta} = \frac{(n_1 - ik_1)}{(n_2 - ik_2)}$$

The perpendicular component of reflectivity is given as

$$r_{\perp}(\theta) = -E_{\perp}\overline{E}_{\perp}$$

Similarly parallel component of reflectivity is given as,

$$r_{//}(\theta) = -E_{//}\overline{E}_{//}$$

and the unpolarized reflectivity is

$$r(\theta) = \left[r_{\perp}(\theta) + r_{//}(\theta)\right]/2$$

Calculating collimated reflectivity at the boundaries is straight forward. For normal incidence, parallel and perpendicular components of reflectivity are equal and the Fresnel formalism yields:

$$r = \frac{(n_2 - n_1)^2 - (k_2 - k_1)^2}{(n_2 - n_1)^2 + (k_2 - k_1)^2} \tag{2.20}$$

Whereas, in order to estimate the diffuse component of reflectivity at boundaries, Equation 2.20 must be integrated over the hemisphere.

Once spectral diffuse and collimated reflectances are estimated by Equation 2.18 and Equation 2.19, spectral reflectance, emittance and absorptance can be calculated as:

$$R_\lambda = R_{d,\lambda} + R_{c,\lambda} \tag{2.21}$$

$$\alpha_\lambda = 1 - R_\lambda \tag{2.22}$$

$$\varepsilon_\lambda = \alpha_\lambda \tag{2.23}$$

Equation 2.23 concludes the model used in this study where spectral emittance of the coating is estimated based on pigment radius, volume fraction, optical properties and matrix or resin thickness, and optical properties.

2.3. Total Emittance and Solar Absorptance

After estimating spectral reflectivity values, total emittance and solar absorptance can be calculated. The total emittance can be represented as:

$$\varepsilon = \frac{\int_0^\infty I_{b,\lambda}(T_a)(1 - R_\lambda)d\lambda}{\int_0^\infty (1 - R_\lambda)d\lambda}$$

where T_a represents the absorber surface temperature. Then the solar absorptance can be calculated as:

$$\alpha_s = \frac{\int_0^\infty I_{s,\lambda}(1 - R_\lambda)d\lambda}{\int_0^\infty (1 - R_\lambda)d\lambda}$$

where $I_{s,\lambda}$ is the incident spectral solar intensity.

2.4. Pigment Distribution

Volume fraction is the ratio of pigments volume to entire volume and can be calculated as:

$$f_v = \frac{4\pi r_p^{\,3}/3}{L_c^{\,3}} \tag{2.24}$$

There is a theoretical limit for volume fraction for a given pigment size as this model is based on spherical particles in a matrix. Particles are assumed to be placed as a simple cubic structure as suggested by Niklasson (2006) and shown in Figure 2.3. When L_c equals to 2r, the highest possible volume fraction value is achieved and the structure becomes compact. For a simple cubic structure, maximum possible volume fraction is 0.52 which is also known as atomic packing factor for simple cubic crystal structure.

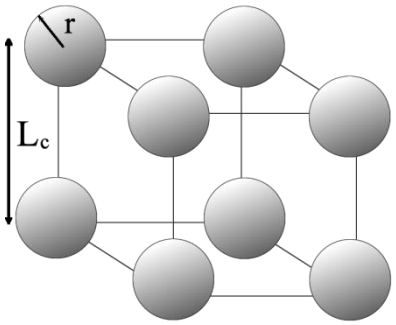

Figure 2.3. Simple cubic alignment of pigments in matrix.

3. MODEL VERIFICATION AND VALIDATION

The developed unified model that can predict the radiative properties of the pigmented coating must be validated or verified before it is used for design of pigmented coatings.

3.1. Verification of Lorenz-Mie theory

The independent scattering model based on Lorentz-Mie theory is verified by comparing the estimated spectral volumetric scattering and extinction cross-sections for different radii to the results presented in Etherden *et al.* (2004). The comparisons presented in Figure 3.1 and 3.2 are for three different radii, lead sulfide (PbS) particles in

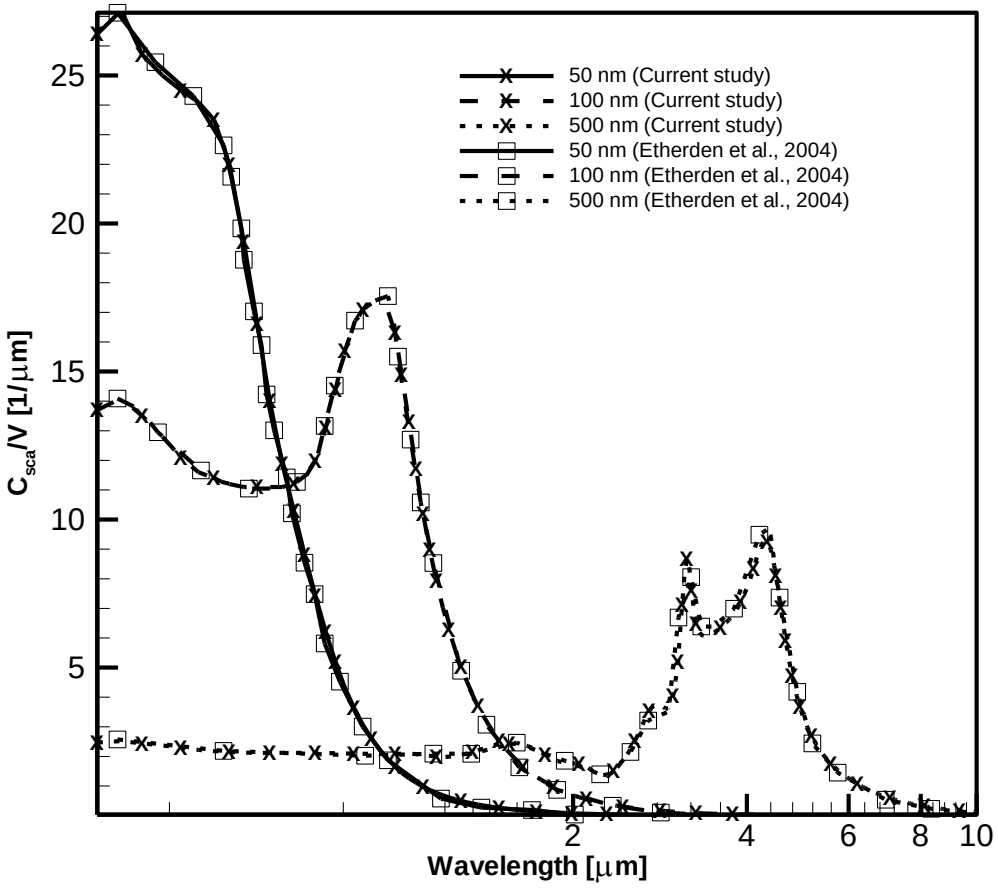

Figure 3.1. Volumetric scattering cross section of 20% lead sulfide (PbS) for three radii.

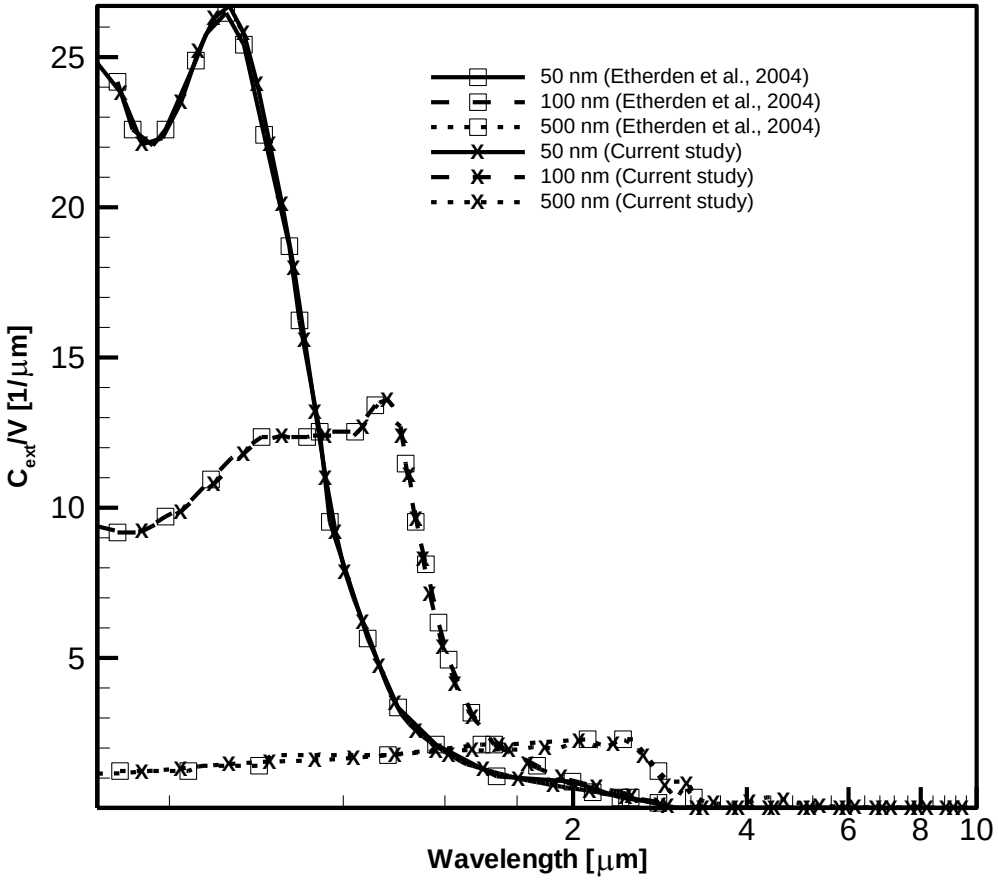

Figure 3.2. Volumetric extinction cross section of 20% lead sulfide (PbS) for three radii.

polybinder with a volume fraction of 20%. An exact match can be observed between the model developed and results presented in Etherden *et al.* (2004), verifying our model.

3.2. T-Matrix Model Verification

T-Matrix model used in this study is based on the research code developed and presented by Mackowski and Mishchenko (2011). Although, the verification of the code is presented in Auger *et al.* (2003), a study is performed to ensure the correct use of the definitions and boundary conditions specified by the input file.

The verification study is carried out by using data from Auger *et al.* (2003) for different linearly aligned compact sphere clusters, indices of refraction of the TiO_2

pigments and the surrounding medium are taken as 2.8 and 1.5, respectively. The variation of volumetric scattering cross section for a wavelength of 0.546 micrometers with respect to particle radius is presented in Figure 3.3. Comparing the agreement between the results presented in Auger *et al.* (2003) and the predicted quantities, it is concluded that use of the code developed by Mackowski and Mishchenko (2011) is verified.

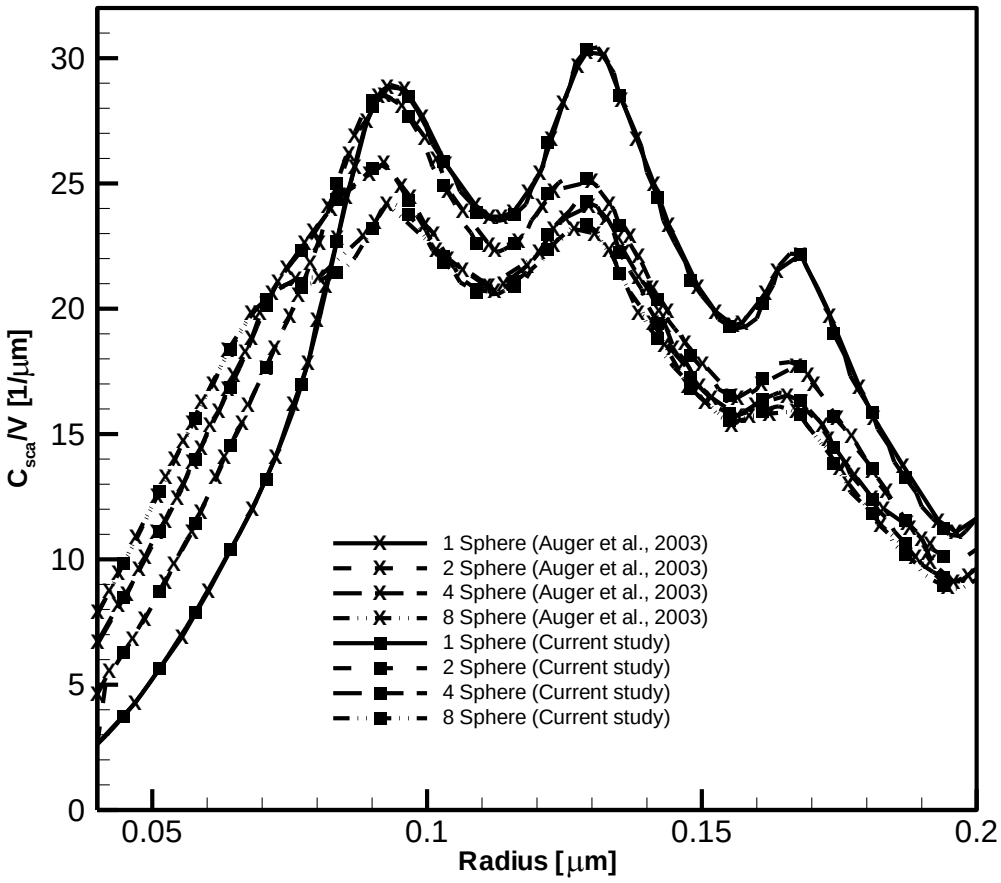

Figure 3.3. Volumetric scattering cross section calculated by T-Matrix.

3.3. T Matrix Geometric Modeling

As mentioned earlier, T-matrix method can consider multiple particles and modeling of dependent scattering in a particle cloud necessitates the simulation of large number of particles. While the number of particles increases, the required computation time also increases significantly. However, it should be noted that the effect of one particle to another becomes negligible beyond a distance and increasing the cluster size further will

not improve the accuracy of the predicted scattering and absorption cross-sections of the cluster. On the other hand, using a small cluster will reduce the computation time, whereas it will reduce prediction accuracy too. In order to understand the optimal cluster size, clusters with different number of particles are modeled and their spectral reflectances with respect to wavelength inspected.

Five different configurations and a single particle are considered as shown in Figure 3.4. Optical properties of coating, with PbS particles at 150 nm radius in polybinder with 2 μm thickness and 0.2 volume fraction applied on copper substrate, are predicted by using the T-Matrix method.

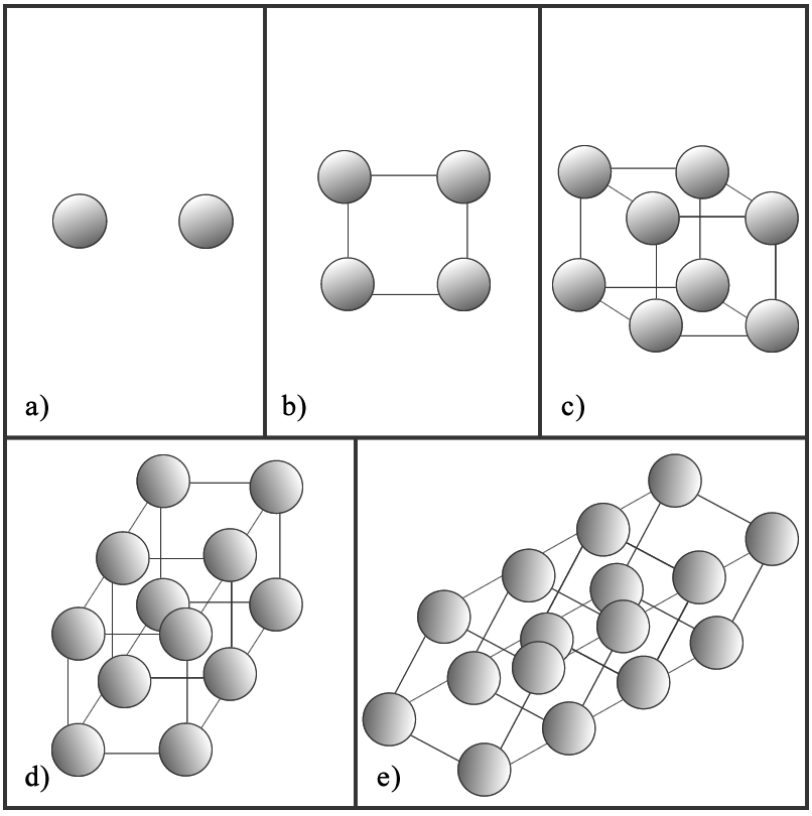

Figure 3.4. Geometric positioning of clusters. (a) 2 particles (b) 4 particles (c) 8 particles (d) 12 particles (e) 16 particles.

A comparison of spectral reflectances predicted by T-Matrix method, for the particle clusters containing different number of particles as shown in Figure 3.4 is presented in Figure 3.5. The spectral reflectance values converge as the number of particles used in the

simulation increases. The predicted reflectance using 8, 12 and 16 particles similar over the entire spectrum and especially in the visible light range. Running time for T-Matrix code using single core of a 2.4 GHz processor for 20 wavelength values from 0.3 to 2.5 micrometer is presented in Table 3.1. PbS particles with 150 nm radius and 0.2 volume fraction at 1 μm thickness is chosen. Considering the significant difference in computation time required by simulations considering 8, 12 and 16 particles, it is concluded that using 8 particles yields the optimal compromise between computation accuracy and efficiency.

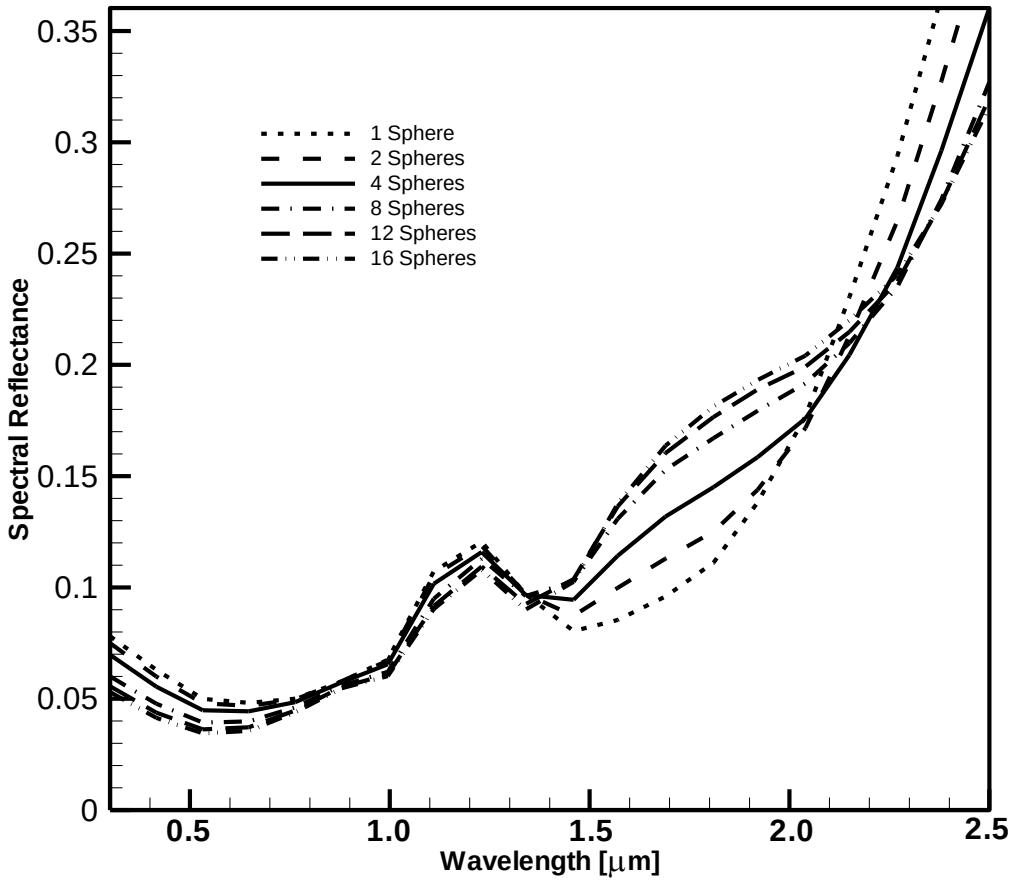

Figure 3.5. Spectral reflectance of different particle clusters

Table 3.1. Running time of T-Matrix code for different sphere clusters presented in Figure 3.4.

Number of spheres	CPU Time (minutes)
1	0.07
2	0.39
4	1.32
8	7.16
12	43.33
16	83.08

3.4. Four Flux Model Validation

A validation study is performed to understand the predictive accuracy of the model outlined in the preceding sections. The experimental data presented in (Vargas and Niklasson, 1997b) is used for the validation study. The measurement used is for a coating designed for radiative cooling purposes, using rutile TiO_2 pigments with 150 nm radius, in a 67 μm thick polymer binder, and the pigment volume fraction is 0.014. The optical properties for the pigment (rutile TiO_2), polymer binder and glass substrate are presented in Figure B.1. The comparisons presented in Figure 3.6 indicate that the model is in good agreement with measured values, validating our model.

3.5. Comparison of Scattering Models

As explained earlier, using different scattering models for predicting radiative properties of pigmented coatings are appropriate for different scattering regimes based on particle size and volume fraction. However, all the previous studies consider only a single model for evaluation of pigmented coatings. A comparative study is performed to quantify the differences between the predictions between models at different scattering regimes.

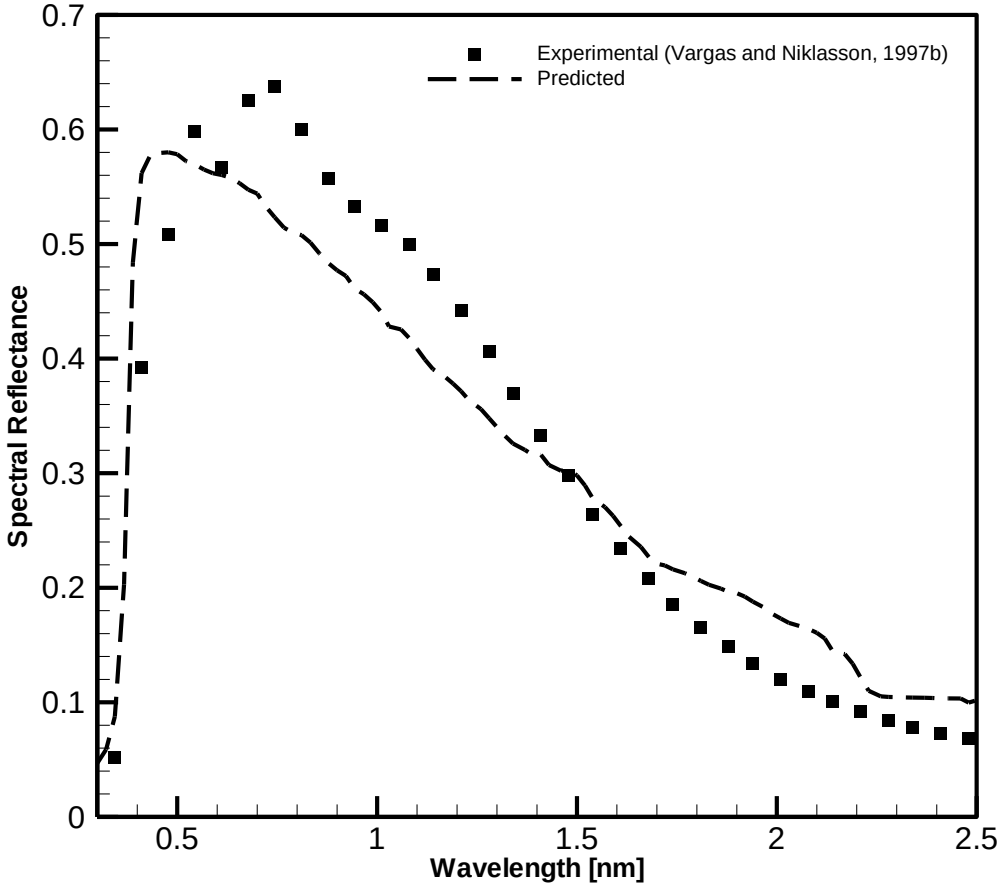

Figure 3.6. Calculated and measured values of rutile TiO_2's reflectivity.

For this purpose the spectral reflectance of a pigmented coating is predicted utilizing effective medium theory (EMT), Lorenz-Mie theory in conjunction with Hartel theory (LMH) and T-matrix method for prediction of radiative properties. Two cases are considered: In the first case PbS pigments with 150 nm radius with a particle volume fraction of 0.1 is considered whereas, in the second case PbS pigments with 50 nm radius with a particle volume fraction of 0.4 is considered. In both cases, the polybinder resin is 1 μm thick. The spectral reflectance of the coating estimated by all three methods are presented with respect to wavelength in Figure 3.7 and Figure 3.8 for the first and second cases, respectively. It should be noted that as the size parameter changes with changing wavelength, along with the governing scattering regime in both cases. The corresponding regimes are also presented in Figure 3.7 and Figure 3.8.

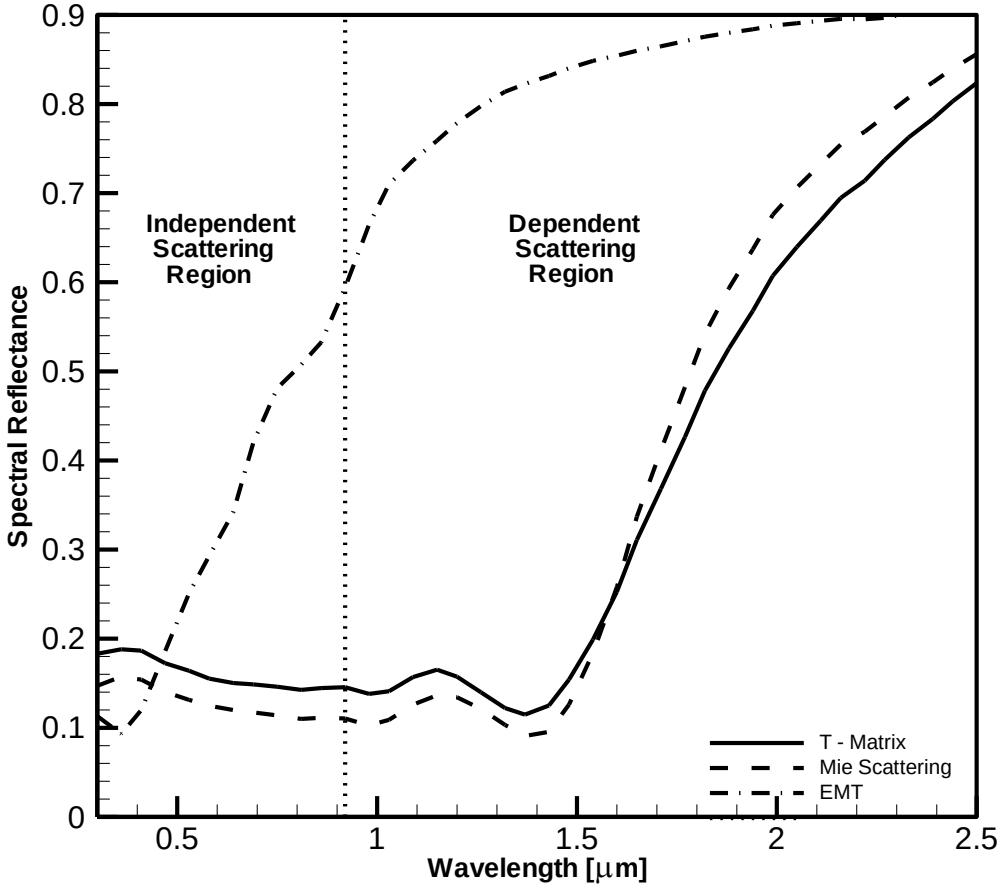

Figure 3.7. Spectral reflectance predicted by different methods for PbS pigments with r_p=150nm, and f_v=0.1 in 1000 nm thick polybinder.

As it could be seen from Figure 3.7, LMH and T-Matrix yield similar results for the case with relatively lower particle volume fraction with larger particle, whereas the EMT deviates significantly from the other solutions. For the case with smaller radius, EMT predicts more accurate results and predicted reflectance values are similar to predictions by LMH or T-Matrix as can be observed from Figure 3.8. Whereas as the volume fraction increases, or the distance between pigments decrease, predictions by LMH deviates from those by T-Matrix method especially for larger wavelengths as observed in Figure 3.8.

LMH method has a good accuracy at visible wavelengths, for considered particle sizes the scattering is independent multiple scattering as can seen from Figure 2.2. On the contrary, emission from the absorber tube is at long wavelengths where size parameter and

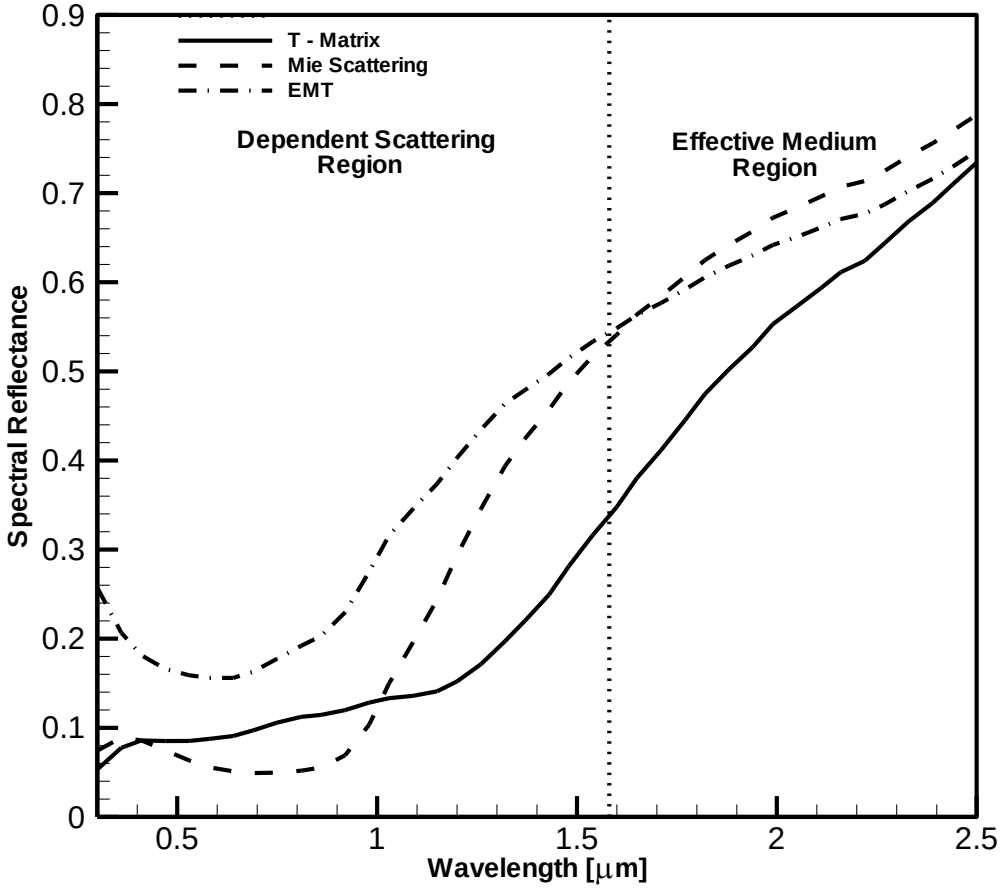

Figure 3.8. Spectral reflectance predicted by different methods for PbS pigments with r_p=50nm, and f_v=0.4 in 1000 nm thick polybinder.

c / λ is small thus scattering region is around at effective medium region or dependent scattering in the scattering regime map.

4. PROBLEM FORMULATION AND OPTIMIZATION

4.1. Problem Formulation

The amount of net heat transfer to the working fluid should be maximized in order to maximize the performance of the concentrating solar thermal system such as a parabolic through system. The absorbers of such systems are subject to concentrated solar irradiation where it is absorbed and transferred to working fluid. The absorbers are usually placed in vacuum tubes to prevent heat loss by convection, and thermal emission from the absorber is only mechanism of heat loss that must be minimized. In this model, convective loss is neglected for simplicity. The net heat flux for the absorber can be defined as:

$$q'' = \int_0^\infty \left[\alpha_\lambda G_{s,\lambda} C_f - \varepsilon_\lambda E_{b,\lambda}(T_a)\right] d\lambda \tag{4.1}$$

Considering that $\alpha_\lambda = \varepsilon_\lambda$, the spectral emittance of an ideal solar coating that maximizes the net heat flux is represented as:

$$\varepsilon_{ideal,\lambda} = \begin{cases} 1 & \lambda \le \lambda_c \\ 0 & \lambda > \lambda_c \end{cases} \tag{4.2}$$

where λ_c represents the cut-off wavelength that depends on the T_a and C_f, for a specific solar irradiation G_λ. In this study, standard solar irradiation data based on ASTM-G173-03 presented in Figure 4.1 is considered.

The cut-off wavelength of the ideal coating can be defined as the wavelength that maximizes the net absorber heat flux defined by Equation 4.1. The change of net absorber heat flux with the cut-off wavelength is shown in Figure 4.2 for five different absorber temperature and concentration factor pairs. The cut-off wavelength for ideal coating for these and four other absorber temperature, concentration factor combinations are presented in Table 4.1. It can be observed in Table 4.1 that cut-off wavelength is a strong function of

absorber temperature, whereas its dependence on concentration factor is weak. Therefore, it will be reasonable to carry out our parametric study over absorber temperature only.

Once the spectral emittance of the ideal coating is defined by Equation 4.2, the design problem can be defined as estimating the design parameters so that the resulting spectral emittance of the pigmented coating will be identical or similar to that of ideal coating. The design parameters for a pigmented coating are pigment material, size and volume fraction, and resin or matrix material and thickness.

The design problem considered in this study is an inverse problem of predicting the cause of a desired event. Considering the formulation presented by Equation 2.23, the design problem for a given absorber temperature, concentration factor, resin thickness,

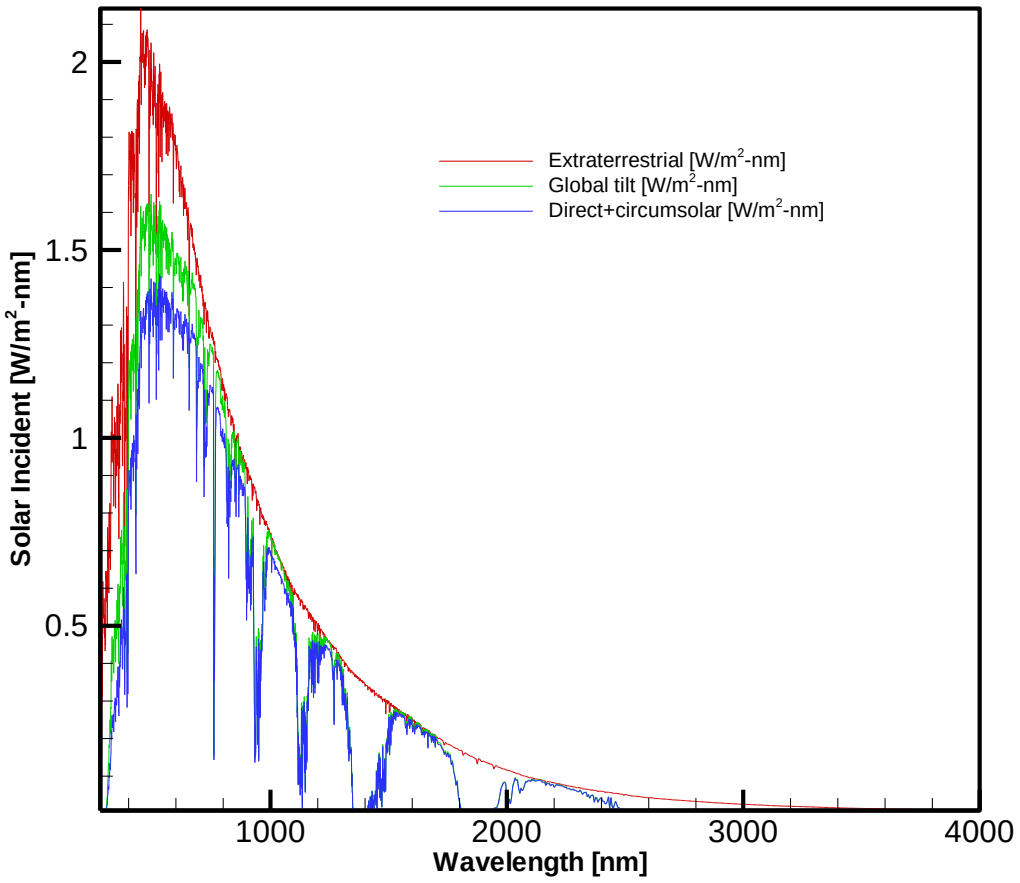

Figure 4.1. Solar irradiation data used in the study (ASTM-G173).

Table 4.1. The cut-off wavelength for ideal coating spectral emittance.

		C_f			
		20	25	30	35
T_a [K]	500	2.48	2.48	2.51	2.51
	600	2.48	2.48	2.48	2.48
	700	2.37	2.41	2.43	2.43

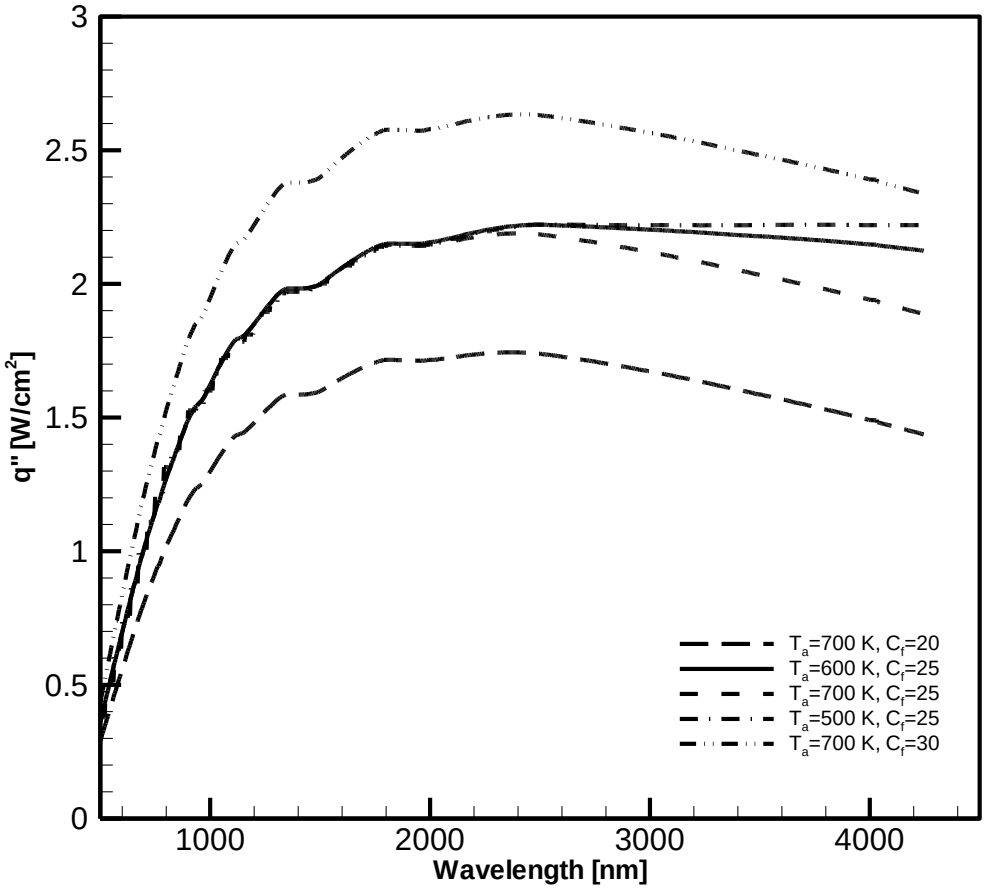

Figure 4.2. The variation net absorber heat flux with cut-off wavelength for coating emittance for different conditions.

pigment and resin material can be formulated as:

$$\varepsilon_{ideal,\lambda}(T_a, C_f) = \varepsilon_\lambda(\chi) \tag{4.3}$$

where the unknown vector is $\chi=[r_p\ f_v]^T$.

Considering the non-linearity of spectral emittance of the pigmented coating, a direct solution for Equation 4.3 is not possible. Non-linear inverse design problems can be solved using optimization techniques as presented by Howell *et al.* (2003) and Daun *et al.* (2002). Optimization techniques can be used for solution of Equation 4.3, if it is formulated as a least squares minimization problem defined by the objective function

$$F(\chi) = \int_0^\infty [\varepsilon_{ideal,\lambda} - \varepsilon_\lambda(\chi)]^2\, d\lambda \tag{4.4}$$

An alternative objective function considers Equation 4.1 and is derived to represent the difference between the net absorber heat for ideal coating and the coating considered. Then, the objective function to be minimized is modified to

$$F(\chi) = \int_0^\infty \{[G_{s,\lambda} C_f - E_{b,\lambda}(T_a)][\varepsilon_{ideal,\lambda} - \varepsilon_\lambda(\chi)]\} d\lambda \tag{4.5}$$

4.2. Optimization Methods

Two optimization methods are used for the solution of the inverse design problem explained by Equation 4.3 through minimization of the objective functions described by Equation 4.4 or Equation 4.5.

4.2.1. Nelder-Mead Simplex Method

First method considered for optimization is Nelder-Mead simplex method (NMSM) (Nelder and Mead, 1965). NMSM, also known as downhill simplex technique, is a simple search algorithm for solving unconstrained, non-linear optimization problems.

In Nelder-Mead algorithm, test points are arranged as a simplex that is a triangle for the two dimensional problem considered. A new test point is generated by extrapolation based on the value of the objective function at tests points. One of the older test points is then replaced by the generated test point. The procedure is repeated until the algorithm converges to a solution. The method does not rely on gradient information, and it might converge to a solution that is not a stationary point. However, the method is used for wide range of applications due to its simplicity. Moreover, it is used for problems with discontinuous gradients. Further information about the method is available at (Lagarias *et al.*, 1998) and (Press *et al.*, 1992).

4.2.2. Quasi Newton Method

The second method used is the Quasi Newton method (QNM). Quasi Newton methods are class of methods that approximate Newton method that finds the stationary points of a function using Hessian matrix that stores the second gradient information for the function through successive iterations using

$$\boldsymbol{\chi}^{k+1} = \boldsymbol{\chi}^{k} - [\mathbf{H}(\boldsymbol{\chi}^{k})]^{-1}[\nabla F(\boldsymbol{\chi}^{k})]$$

Although, Newton method is known to have a high convergence rate as it uses the second gradient information, computation of the Hessian matrix is usually expensive. The QNM overcomes this problem by approximating the Hessian matrix using successive first gradient information. In this study, Broyden-Fletcher-Goldfarb-Shanno (BFGS) algorithm is used where the solution is formulated as

$$\boldsymbol{\chi}^{k+1} = \boldsymbol{\chi}^{k} + \gamma^{k}\mathbf{p}^{k}$$

where γ^{k} is the search step size and

$$\mathbf{p}^{k} = -[\mathbf{B}^{k}][\nabla F(\boldsymbol{\chi}^{k})]$$

and the matrix $\mathbf{B}^{k}$ approximates the inverse of Hessian, $[\mathbf{H}(\boldsymbol{\chi}^{k})]^{-1}$, and it can be estimated from the following recursive relation

$$\mathbf{B}^{k+1} = \mathbf{B}^{k} + \frac{[(\gamma^{k}\mathbf{p}^{k})^{\mathrm{T}}\mathbf{y}^{k} + (\mathbf{y}^{k})^{\mathrm{T}}\mathbf{B}^{k}\mathbf{y}^{k})][(\gamma^{k}\mathbf{p}^{k})^{\mathrm{T}}(\gamma^{k}\mathbf{p}^{k})^{\mathrm{T}}]}{[(\gamma^{k}\mathbf{p}^{k})^{\mathrm{T}}\mathbf{y}^{k}]^{2}} - \frac{\mathbf{B}^{k}\mathbf{y}^{k}(\gamma^{k}\mathbf{p}^{k})^{\mathrm{T}} + (\gamma^{k}\mathbf{p}^{k})(\mathbf{y}^{k})^{\mathrm{T}}\mathbf{B}^{k}}{(\gamma^{k}\mathbf{p}^{k})^{\mathrm{T}}\mathbf{y}^{k}}$$

where

$$\mathbf{y}^{k} = \nabla F(\boldsymbol{\chi}^{k+1}) - \nabla F(\boldsymbol{\chi}^{k}))$$

Derivation and further information about the method is available in Avriel (2003) and Byrd *et al.* (1999).

5. RESULTS AND DISCUSSION

This study aims at optimizing spectrally selective coatings for concentrated solar-thermal applications where the objective is to maximize the energy harvesting from sun, unlike the case for the validation problem. Integrated form of Equation 4.1 can be presented as

$$q'' = \alpha_s C_f G_s - \varepsilon\sigma T_a^4 \tag{5.1}$$

In order to maximize the net heat flux received by absorber, high solar absorptance is desired along with low total emittance. Achieving high solar absorptance is possible by using dark-black pigments with relatively higher extinction index such as lead sulfide (PbS), carbon (C) and nickel (Ni). Therefore, these pigments are considered for the optimization study along with a polymer binder.

Optimization algorithms are first tested considering the case where T_a=700 K, C_f =35, using PbS pigments with 1 μm thick polymer binder using the objective function presented in Equation 4.5. Although it is not required for the solution, the variation of the objective function throughout the solution domain is estimated and plotted as shown in Figure 5.1 to aid evaluation of the optimization methods. Moreover, the unified model is used during the estimation of the spectral emittance, utilizing the criteria presented in (Brewster and Tien, 1982) and (Howell *et al.*, 2011) at all wavelengths of each search point to select the model (LMH, T-matrix method, or EMT) to be used. It can be observed from Figure 5.1 that the solution lies around f_v=0.2-0.4 and between r_p=150-220 nm.

The first method considered is the NMSM. The method is tested using different initial guesses. While NMSM converges for all, only one of these is presented in Figure 5.1. Considering the mild gradient in the topology, the algorithm fluctuates around the solution r_p=181 nm, and f_v=0.27, converging after 99 objective function evaluations. A similar test is performed for the QNM. Different initial guesses and different step size parameters are used for the solution of the same problem. The maximum step size for

which QNM converges to the same solution (r_p=181 nm, and f_v=0.27), independent of the initial guess is determined and this step size is used in further solutions. The QNM takes a more direct route to the minimum point and converges after 66 function evaluations, using approximately two thirds the computation time NMSM uses.

Based on these results, it is concluded that both NMSM and QNM are reliable and robust methods for solution of the optimization problem considered in this study, with QNM having superior convergence. Therefore, QNM is used in the rest of the study.

Solution of the design problem using objective function defined by Equation 4.5, for other temperatures, using different pigment materials (PbS, C, Ni) are estimated for a

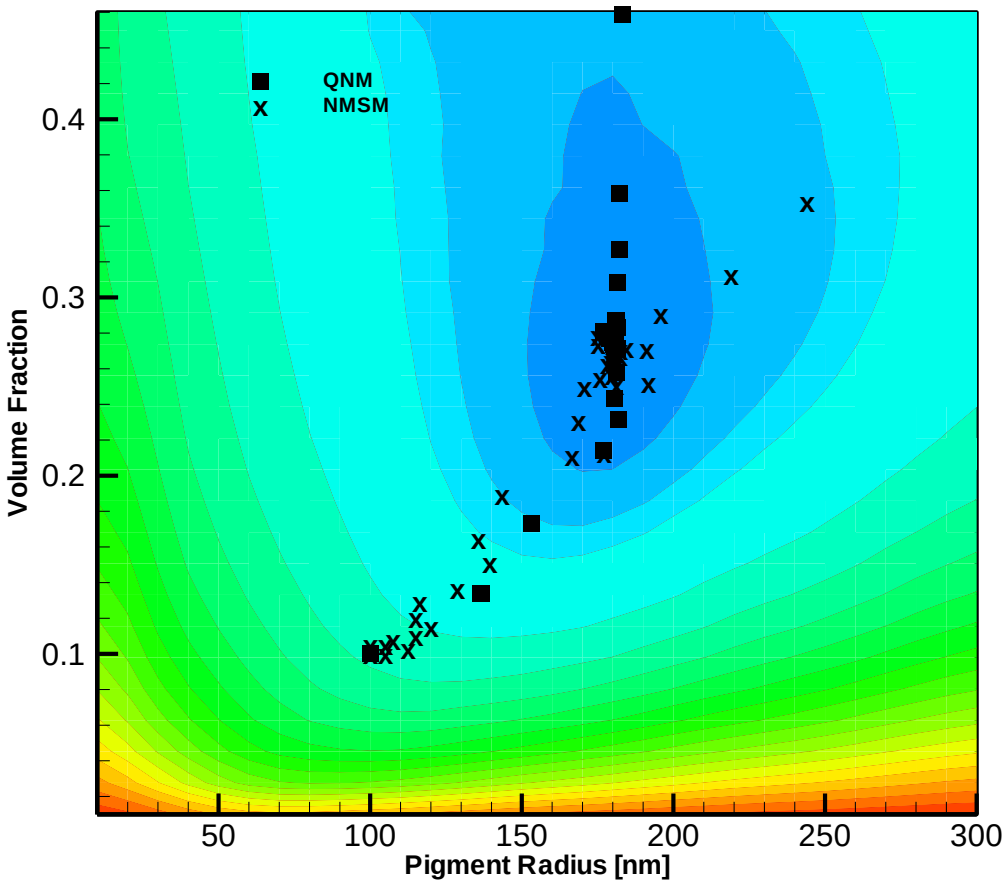

Figure 5.1. Variation of objective function for the solution domain for T_a=700 K, C_f=35, t=1 μm, and iterations for the NMSM and QNM.

concentration factor of 35 by using QNM. A summary of the results are presented in Table 5.1. It can be observed that as the absorber temperature changes, the optimal parameters defining the optimal pigmented coating changes significantly. It is clear from results presented in Table 5.1 that the operation temperature must be considered while designing the absorber coating to maximize system performance.

The solar absorptance of coatings with all three pigments are similar, whereas the total emittance of carbon is larger than the others and the PbS has the smallest total emittance. This difference reflects into the difference in the absorber net heat flux shown in Figure 5.2. Coating with PbS results in higher absorber net heat flux, while coating with nickel results in the least net absorber flux. As the absorber temperature increases from 600 to 700 K, the difference between net absorber heat flux of Ni, PbS and carbon pigmented coatings increases from 1% to 4%. While increasing absorber temperature increases emission and hence decreases net heat flux, it is clear that any thermodynamic cycle operating on higher temperature will have higher efficiency improving the overall performance.

The spectral emittance of the pigmented coatings indicated in Table 5.1 are presented in Figures 5.3 and 5.4, for absorber temperatures of 600 K and 700 K respectively, along

Table 5.1. Summary of optimal parameters for spectrally selective coating for concentrating solar thermal systems using objective function in Equation 4.5.

T_a [K]	Pigment Material	r_p [nm]	f_v	α_s	ε
500	PbS	250	0.52	0.945	0.090
	Ni	256	0.52	0.927	0.098
	C	288	0.52	0.968	0.114
600	PbS	206	0.36	0.930	0.070
	Ni	205	0.34	0.878	0.070
	C	250	0.35	0.937	0.102
700	PbS	181	0.27	0.922	0.030
	Ni	173	0.27	0.874	0.064
	C	221	0.31	0.932	0.107

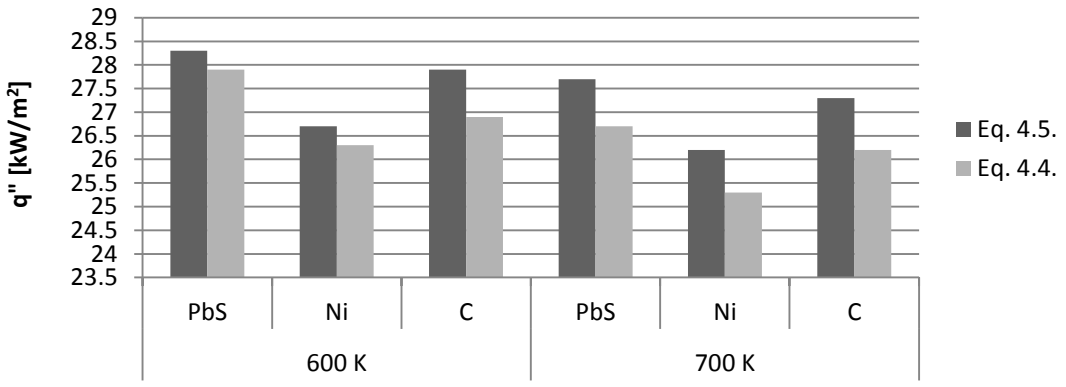

Figure 5.2. Absorber net heat flux for C_f=35, t=1 μm for different materials and temperatures.

with the spectral emittance of the ideal coating described earlier. As it could be seen from Figures 3.7 and 3.8, LMH model estimate a higher spectral reflectance than unified model for long wavelengths, especially for carbon. While switching to EMT at longer wavelengths, a discontinuous behavior appears in carbon around 8 μm wavelength in Figure 5.3. This behavior is less significant at other pigments due to their optical properties. Considering the objective function defined by Equation 4.5, the coating with PbS pigments follows the behavior of the ideal coating more closely than the others and it can be concluded that it is the best pigment material for the problem considered.

Solution of the design problem using objective function defined by Equation 4.4 is considered next. Table 5.2 presents a summary of the results using Equation 4.4. The optimal solutions presented in Table 5.1 and Table 5.2 are different, resulting in slightly different solar absorptance and total emittance values. In general the both solar absorptance values and total emittance values presented in Table 5.1 are larger. Considering that the ideal coating's solar absorptance is 0.989, and its total emittance is 0.01; this is somewhat expected considering that minimizing the objective function given in Equation 4.5 emphasizes more on minimizing the difference from the ideal coating spectral emittance on shorter wavelengths where most of the radiant exchange takes place, resulting in larger solar absorptance. This is also observed in Equation 5.1. As the coefficient of solar absorptance in Equation 5.1 is larger, it has a more significant influence on net absorber heat flux, and optimization using objective function in Equation 4.5

focuses on minimizing solar absorptance more than total emittance. On the contrary, Equation 4.4 tries to match the ideal coating spectral emittance regardless of the wavelength. Therefore, minimizing the solar absorptance and total emittance is considered with equal importance leading to better total emittance values.

It can be observed from Figure 5.2 that the net absorber heat fluxes for coatings optimized by minimizing Equation 4.5 yields slightly higher values than the coatings optimized by minimizing Equation 4.4. This trend is consistent with the discussion above.

The spectral emittance for optimal coatings designed by optimizing objective functions presented in Equation 4.4 and Equation 4.5, using PbS pigments, for T_a=700 K, C_f=35, and t=1 μm are compared with the ideal coating in Figure 5.5. While the spectral

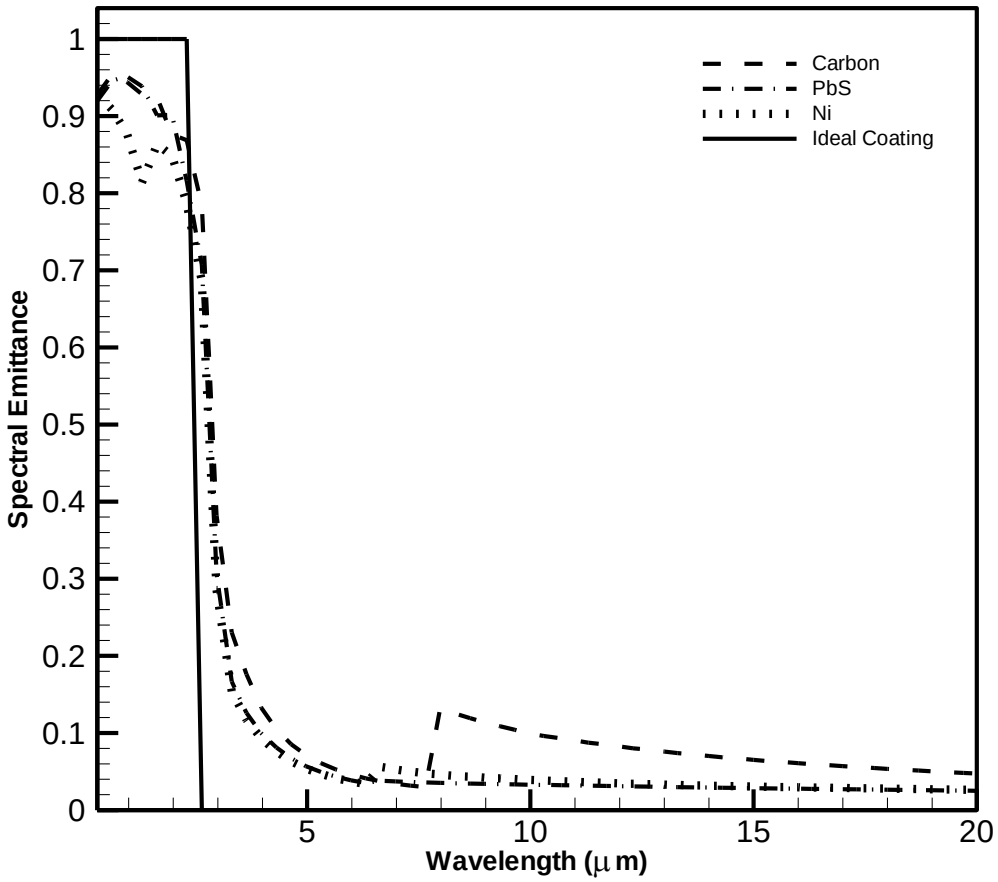

Figure 5.3. Optimal spectral emittance of different materials at T_a=600 K, C_f=35, t=1 μm, using Equation 4.5.

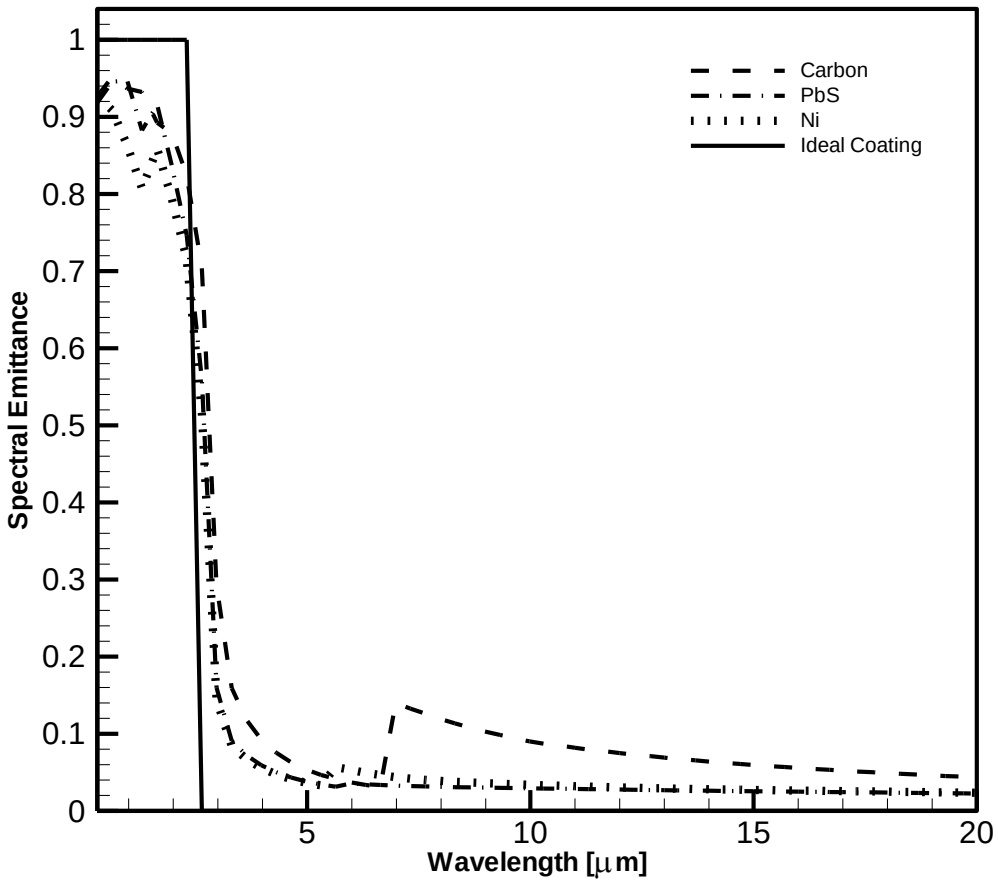

Figure 5.4. Optimal spectral emittance of different materials at T_a=700 K, C_f=35, t=1 μm, using Equation 4.5.

Table 5.2. Summary of optimal parameters for spectrally selective coating for concentrating solar thermal systems using objective function in Equation 4.4.

T_a [K]	Pigment Material	r_p [nm]	f_v	α_s	ε
600	PbS	200	0.35	0.922	0.064
	Ni	207	0.33	0.876	0.069
	C	238	0.35	0.931	0.122
700	PbS	178	0.25	0.911	0.051
	Ni	155	0.25	0.862	0.059
	C	225	0.31	0.929	0.113

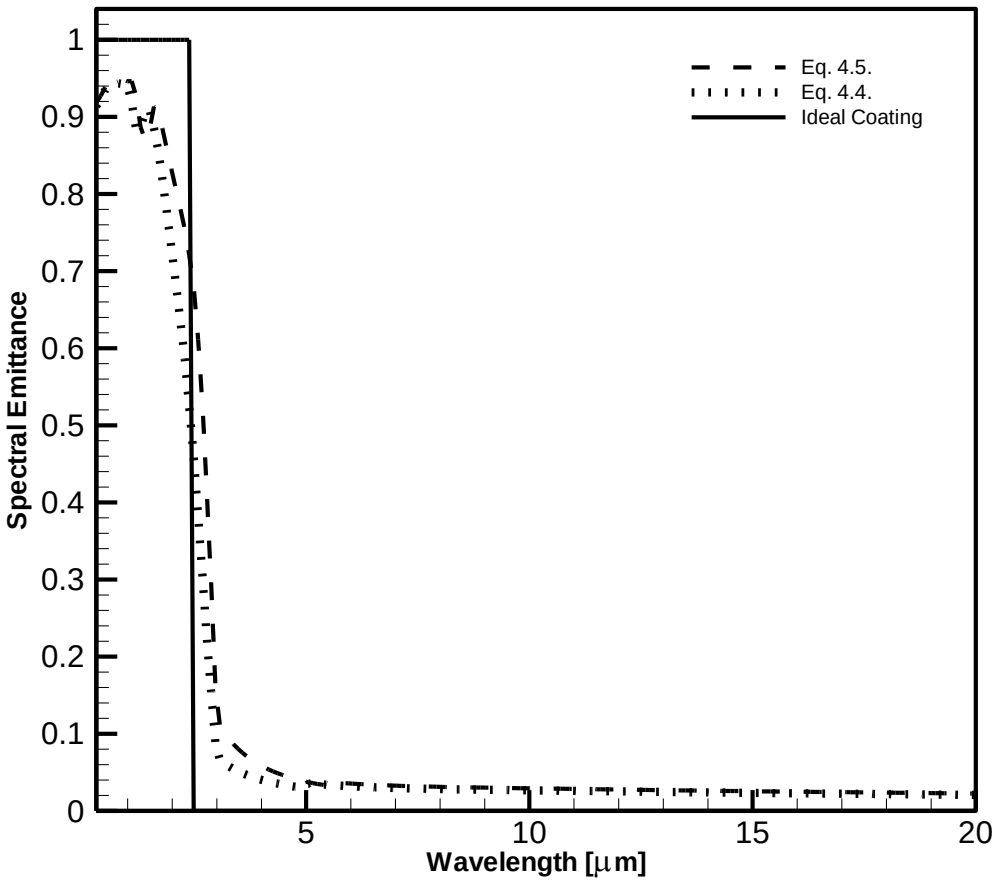

Figure 5.5. Optimal spectral emittance of coatings with PbS pigments at T_a=700 K, C_f=35, t=1 μm, using Equation 4.4 and Equation 4.5.

emittance of both coatings are very similar, the coating optimized by Equation 4.5 follows the ideal coating spectral emittance more closely on shorter wavelengths where solar radiation emits, whereas the spectral emittance of coating optimized by Equation 4.4 follows the ideal coating spectral emittance closer on longer wavelengths.

LMH model estimate spectral reflectance successfully around independent and multiple scattering zone, but at long wavelengths, scattering occurs in either dependent or effective medium zone due to small c/λ and/or small size parameter values. Emittance has an important effect on efficiency and as it could be seen from Figure 4.2, it is dominant at long wavelengths therefore to estimate emittance accurately, effective medium theory and

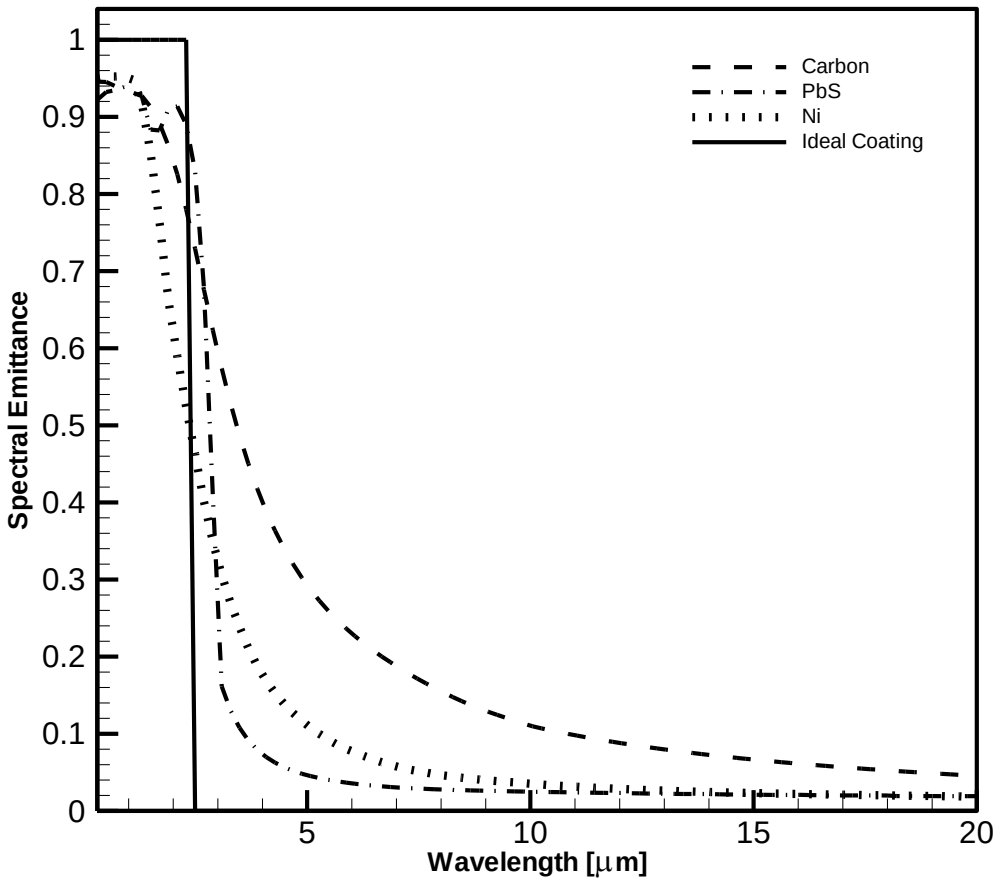

Figure 5.6. Optimal spectral emittance of different materials at T_a=700 K, C_f=35, t=1 μm, using Equation 4.5 and LMH only.

T-matrix model is used. Many of the earlier studies such as Etherden *et al.* (2004), Baneshi et al. (2009), and Yalçın and Ertürk (2011) estimated spectral reflectance with LMH model only. A comparison is presented here with results from Yalçın and Ertürk (2011)and result is presented at Figure 5.6 where spectral emittance graph at long wavelengths differs from this study.

Etherden *et al.* (2004) suggested that, optimal radii for pigmented coatings are around 100 and they also claimed if further optimization study is made, exact optimum radii could be found between 100 and 500 nm in each case.(for C, PbS and Ni at different temperatures in polybinder). The optimal radii estimated are in agreement with their suggested range. Etherden *et al.* (2004) estimated absorptance and emittance for coating

with PbS particles at 200 nm radius and 0.2 volume fraction, as 0.91 and 0.11, respectively, which is optimal value presented in the study. In the current study, by using particles with 181 nm radius at 0.27 volume fraction, absorptance and emittance is estimated as, 0.922 and 0.03, respectively.

Using LMH model only, optimum particle radius and volume fraction for PbS particles at 700 K surface temperature in polybinder are predicted as 173 nm and 0.29, respectively. These values are estimated as 181 nm and 0.27, respectively, using the unified model. The change in the solar absorptance and total net heat flux are 0.8 % and 1 %, respectively. Although, these changes might appear minor total emittance value changes significantly. The unified model estimates emittance as 0.03, where LMH predicts it as 0.05. Considering the similarity in predicted pigment size and concentrations by both models, it can be concluded that using LMH model is acceptable to predict optimum pigment size and concentration for spectrally selective absorbing coatings. Similarly, LMH model is capable of estimating absorptance where it dominates in solar wavelengths, however to estimate optical properties at long wavelengths, a unified model is needed in order to perform more accurate estimation of properties.

6. CONCLUSIONS AND FUTURE WORK

6.1. Conclusions

Inverse design of spectrally selective pigmented coatings is presented for concentrating solar thermal applications. A unified model is developed first, for predicting the radiative transport properties of pigmented coatings. Lorenz-Mie theory in conjunction with Hartel theory is used to predict radiative properties for independent scattering with multiple scattering effects, whereas T-matrix is used for dependent scattering, along with effective medium theory for very small pigments. Once the radiative properties are estimated, the spectral emittance of the coating is calculated by four flux method.

Ideal coating behavior depends strongly on working conditions of the system such as absorber temperature, and concentrating factor. The design problem can be formulated as estimating the design parameters, for achieving the ideal coating behavior. Such a design problem is an inverse problem where a system that exhibits a desired behavior under known conditions is predicted. Moreover, the design problem is a non-linear inverse problem due to highly non-linear dependence of coating behavior on design parameters. Therefore, the solution of the non-linear inverse design problem is achieved through optimization techniques. The optimization problem formulated as minimization problem of an objective function.

Two optimization methods, Nelder-Mead simplex method and Quasi Newton method are tested in this study. While both methods yield identical results, the convergence of the Quasi Newton method was superior to that of Nelder-Mead simplex method. Similarly, two objective functions are considered. Optimizing the objective function that takes energy exchange into account results in coatings with higher net absorber heat flux than the objective function considering the least squares minimization of difference from the ideal coating behavior.

It was found that the solar absorptance of coatings with lead sulfide pigments is superior to those with nickel and carbon pigments. While the solar absorptance of lead

sulfide pigmented coatings is similar to that of carbon pigments, they have significantly lower total emittance. Therefore, the net heat flux for absorber with lead sulfide pigmented coatings is the maximum among the three. The optimal pigment radius and volume fraction is strongly dependent on prescribed absorber temperature. Therefore, pigmented coatings must be designed considering the operating conditions of the system.

6.2. Recommendations for Future Work

The design method proposed in this study can easily be extended to designing a multi-layer coating considering each layer's optical property. These layers might comprise of multiple layers of pigmented coatings, protective layers, or antireflection layers. The effects of using a vacuum tube of different thickness or properties can also be included in the analysis.

Although a single spectral solar irradiance is used for this study, Another possibility is considering seasonal or annual solar irradiance to optimize for seasonal or annual energy production by modifying the objective function. Based on the flexibility of the design approach presented here, the models developed in this study could be used to handle various design scenarios.

In the current study, only first law efficiency for a defined absorber temperature is considered by defining the ideal coating that maximizes the net heat flux to the absorber, which in turn maximizes the collector efficiency based on the first law of thermodynamics. The design can be extended to consider second law efficiency, where prediction of the absorber temperature can be included in the analysis. Then an optimization study by considering thickness of coating can be performed that includes conductive heat transfer in coating as well as radiative heat transfer. While such a study can be performed for single layer coating similar to the one considered in this study, multiple layers can also be considered.

The inverse design concept and the unified model developed could also be used for different applications. By using nano-particles embedded in coatings, spectrally selective behavior for various radiative thermal management applications such as for building walls,

satellites and or window glasses can be achieved. Each of these systems have their distinct limitations and the study can be extended to incorporate designing for these applications considering these limitations.

The developed tool in this study is not only capable of thermal design of radiative systems. It can also be further developed to an optical design tool, so that altering the nano-particle size, and concentration of the coatings will result in different lightning or coloring options. Moreover, if spheroid nano-particles are used, by adjusting the orientation of these spheroid particles, the lighting or color can be adjusted.

APPENDIX A: FORMULATION OF HARTEL THEORY

Hartel theory is used to model multiple scattering at independent scattering region. By using

$$p(\cos\theta) = \frac{2}{x^2 Q_{ext}} \left\{ \left| S_1(\cos\theta) \right|^2 + \left| S_2(\cos\theta) \right|^2 \right\}$$

And by integrating Equation 2.16, σ_c becomes

$$\sigma_c = \frac{1}{2\omega_0} \cdot (\omega_0 + \sum_{i=1}^{\infty} \omega_i \cdot g_i)$$

Where particle albedo ω_0 is defined as:

$$\omega_0 = Q_{sca} / Q_{ext}$$

And w_i coefficients could be obtained as follow

$$\omega_i = \frac{2i+1}{x^2 Q_{ext}} \cdot (\sum_{n=1}^{\infty} \gamma_n \sum_{m=1}^{n} \gamma_m \frac{W_{nm}\eta_{nmi} I_{nmi} + V_{nm}\nu_{nmi} J_{nmi}}{1+\delta_{nm}})$$

Where

$$\gamma_n = \frac{2n+1}{n(n+1)}$$

$$W_{nm} = \mathrm{Re}\left\lfloor a_n a_m^{\,*} + b_n b_m^{\,*} \right\rfloor$$

$$V_{nm} = \mathrm{Re}\left\lfloor a_n b_m^{\,*} + b_n a_m^{\,*} \right\rfloor$$

$$I_{nmi} = \int_{-1}^{1} [\pi_n \pi_m + \tau_n \tau_m] P_i(\mu) d\mu$$

$$J_{nmi} = \int_{-1}^{1} [\pi_n \tau_m + \tau_n \pi_m] P_i(\mu) d\mu$$

With

$$\pi_n = \frac{dP_n}{d\mu}$$

$$\tau_n = \mu \frac{dP_n}{d\mu} - (1-\mu^2) \frac{d^2 P_n}{d\mu^2}$$

I_{nmi} and J_{nmi} were calculated by Chu and Churchill and given as

If n+m-i is even:

$$I_{nmi} = [n(n+1) + m(m+1) - i(i+1)]^2 \frac{(n+i-m)!(m+i-n)!(n+m-i)!}{(n+m+i+1)!} \times \left\{ \frac{[(n+m+i)/2]!}{[(n+m-i)/2]![(-n+m+i)/2]![(n-m+i)/2]!} \right\}^2$$

and $J_{nmi}=0$. Whereas, if n+m-i is odd; $I_{nmi}=0$ and

$$J_{nmi} = [(n+m-i)(n+i-m+1)(m+i-n+1)] \times \frac{(n+i-m+1)!(m+i-n+1)!(n+m-i-1)!}{(n+m+i+1)!} \times \left\{ \frac{[(n+m+i+1)/2]!}{[(n+i-m+1)/2]![(-n+m+i+1)/2]![(n+m-i-1)/2]!} \right\}^2$$

If $0 \le n+m-i \le 2m$, then $\eta_{nmi}=1$, whereas if otherwise $\eta_{nmi}=0$.

Likewise

$$\nu_{nmi}=1 \text{ if } 1 \le n+m-i \le 2m+1$$

$$\nu_{nmi}=0 \text{ otherwise}$$

$$g_i = \int_0^1 P_i(\mu)d\mu = (-1)^{(i-1)/2} \cdot \frac{(i!!)^2}{i(i+1)i!} \text{ when i is odd,}$$

$$g_i = 0 \text{ when i is even.}$$

For diffuse radiation, phase function must be generalized to handle various incident and scattered directions which are shown by θ‘ and θ respectively.

$$p(\mu,\mu') = \sum_{n=0}^{\infty} \omega_n P_n(\mu) P_n(\mu')$$

Diffuse radiation is given as:

$$\sigma_d = \frac{\int_0^1 \int_{-1}^1 I(z,\mu')\, p(\mu,\mu') d\mu' d\mu}{\int_{-1}^1 \int_{-1}^1 I(z,\mu')\, p(\mu,\mu') d\mu' d\mu}$$

For isotropic radiation, intensity doesn’t depend on polar angle so diffuse forward scattering ratio could be found as:.

$$\sigma_d \cong \sigma_d^{(i)} = \frac{1}{2\omega_0} \cdot (\omega_0 + \sum_{n=1}^{\infty}{}' \omega_n \cdot g_n^2)$$

In Hartel theory forward diffuse intensity is given as:

$$I(z,\mu) = \sum_{k=1}^{\infty} Q_k(z) f_k(\mu)$$

Where

$$f_k(\mu) = \frac{1}{4\pi} \sum_{n=0}^{\infty} (2n+1) \left[\frac{\omega_n / \omega_0}{2n+1} \right]^k P_n(\mu)$$

In original Hartel theory Q_k is given as:

$$Q_k(z) = \left[(\alpha z)^k / k! \right] e^{-(\alpha+\beta)z}$$

To use extended version of Hartel's theory Q_k is given as:

$$Q_k(z) = p_k(z) e^{-(\alpha+\beta)z}$$

Where

$$p_k(\tau) = F_k \left[1 - e^{-(\xi_k - 1)\tau} \right] + \sum_{i=1}^{k-1} G_{i,k} \left[e^{-(\xi_k - 1)\tau} - e^{-(\xi_i - 1)\tau} \right]$$

$$\xi_k = 2 \left\{ \left(1 + \sum_{n=1}^{\infty} (2n+1) g_n [\psi_n]^k \right) \left[1 + 2 \left(\frac{\omega_1}{3\omega_0} \right)^k + 2 \sum_{n=2}^{\infty} (2n+1) h_n [\psi_n]^k \right]^{-1} \right\}$$

$$\psi_n = \frac{\omega_n / \omega_0}{2n+1}$$

$$\frac{dQ_1}{dz} = aQ_0 - \xi_1 (\alpha + \beta) Q_1$$

$$\frac{dQ_k}{dz} = \xi_{k-1} \alpha Q_{k-1} - \xi_k (\alpha + \beta) Q_k$$

$$F_k = \omega_0 \frac{\xi_{k-1}}{\xi_k - 1} F_{k-1}$$

$$G_{k-1,k} = \omega_0 \frac{\xi_{k-1}}{\xi_k - \xi_{k-1}} \left[F_{k-1} - \sum_{i=1}^{k-2} G_{i,k-1} \right]$$

$$G_{i,k} = \omega_0 \frac{\xi_{k-1}}{\xi_k - \xi_i} G_{i,k-1}$$

With initial values:

$$F_1 = \frac{\omega_0}{\xi_1 - 1}$$

$$G_{1,2} = \frac{\omega_0}{\xi_2 - \xi_1} F_1$$

By using Hartel theory diffuse radiation could be found by:

$$\sigma_d(z) = \frac{\left(\sigma_d^{(i)} + \frac{1}{2} \sum_{n=1}^{\infty}{}' \frac{c_n(z) g_n}{c_0} \cdot \left[1 + \frac{\omega_n X_{nn}}{\omega_0} \right] + \frac{1}{2} \sum_{n=1}^{\infty}{}' \frac{\omega_n g_n}{\omega_0} \sum_{m=2}^{\infty}{}'' \frac{c_m(z) X_{nm}}{c_0} \right)}{1 + \sum_{n=1}^{\infty}{}' \frac{c_n(z) g_n}{c_0}}$$

Where

$$\chi_{nm} = \frac{1}{2^{n+m}} \sum_{k=0}^{n/2} \sum_{j=0}^{m/2} \frac{(-1)^{j+k}}{[n+m+1-2(j+k)]} \frac{(2n-2k)!(2m-2j)!}{(n-k)!\,k!\,(n-2k)!\,(m-j)!\,j!\,(m-2j)!}$$

$$c_n(z) = \frac{2n+1}{4\pi} \sum_{k=1}^{\infty} Q_k(z) \left[\frac{\omega_n / \omega_0}{2n+1} \right]^k$$

$$\xi(z) = 2 \left[\left(1 + \sum_{n=1}^{\infty}{}' \frac{c_n(z)}{c_0(z)} \cdot g_n \right) \left(1 + \frac{2c_1(z)}{3c_0(z)} + 2 \sum_{n=2}^{\infty}{}'' \frac{c_n(z)}{c_0(z)} X_{n1} \right)^{-1} \right]$$

APPENDIX B: OPTICAL DATA

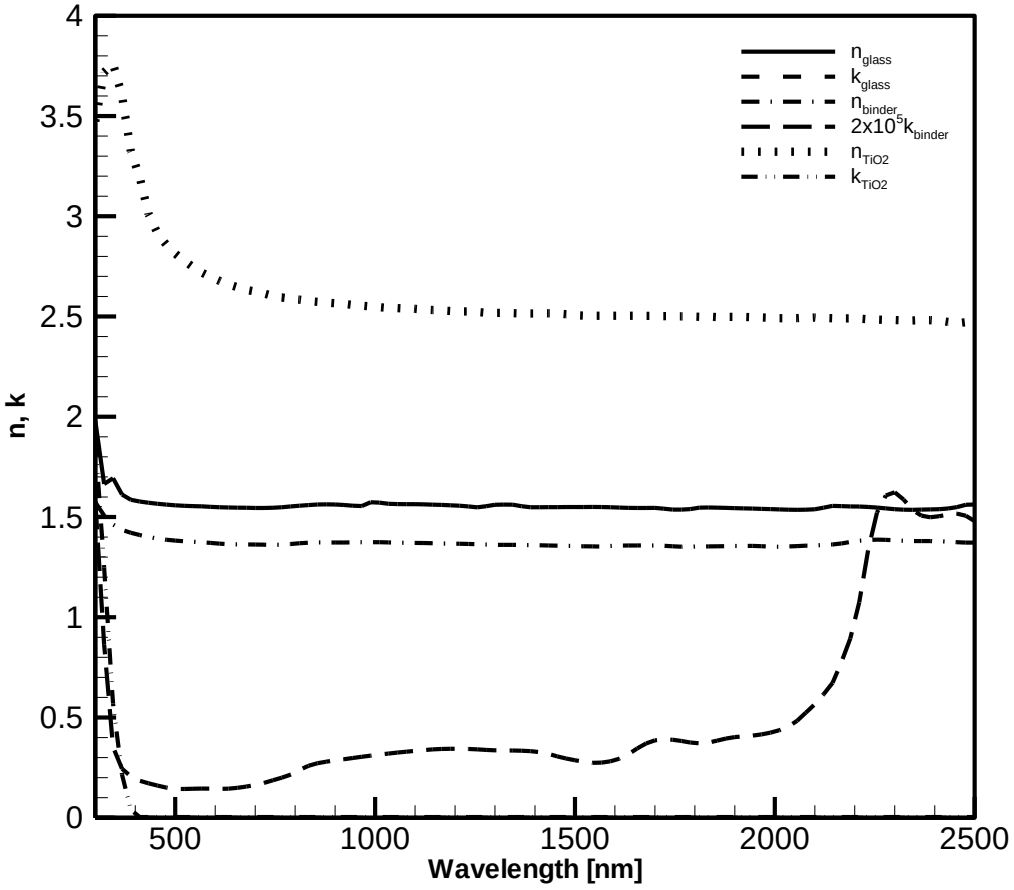

Figure B.1. Optical properties of pigments that are used in model validation (Vargas, 1997).

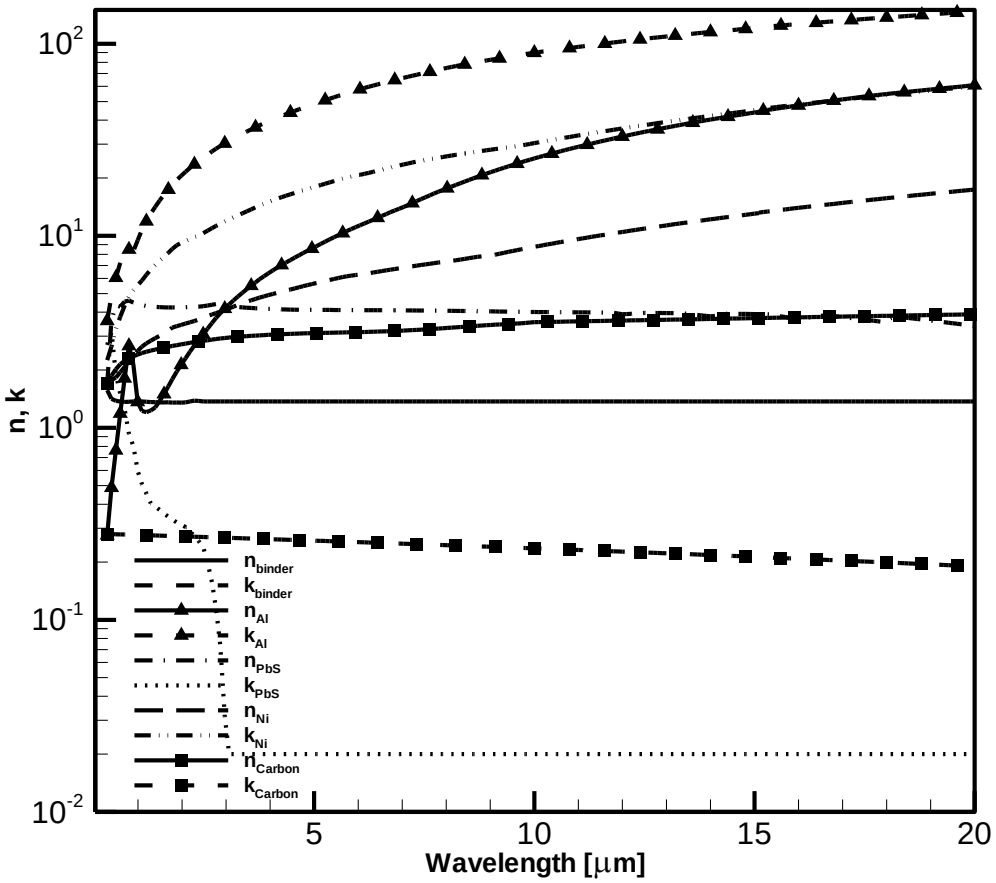

Figure B.2. Optical properties of pigments that are used in optimization (Vargas, 1997).

REFERENCES

American Society for Testing and Materials (ASTM) Terrestrial Reference Spectra, 2008, ASTM G-173-03.

Avriel M., 2003, *Nonlinear Programming Analysis and Methods*, Dover, New York.

Auger J. C., R. G. Barrera, and B. Stout, 2003, "Scattering Efficiency of Clusters Composed by Aggregated Spheres", *Journal of Quantitative Spectroscopy & Radiative Transfer*, Vol. 79-80 , pp. 521-531.

Baneshi M., S. Maruyama, H. Nakai, and A. Komiya, 2009, "A New Approach to Optimizing Pigmented Coatings Considering both Thermal and Aestetic Effects", *Journal of Quantitative Spectroscopy and Radiative Transfer*, Vol. 110, pp. 192-204.

Baneshi M., S. Maruyama, and A. Komiya, 2011, "Comparison between Aesthetic and Thermal Performances of Copper Oxide and Titanium Dioxide Nano Particulate Coatings", *Journal of Quantitative Spectroscopy and Radiative Transfer*, Vol. 112, pp. 1197-1204.

Bohren C.F., 1986, "Applicability of Effective Medium Theories to Problems of Scattering and Absorption by Nonhomogeneous Atmospheric Particles", *Journal of the Atmospheric Sciences*, Vol. 43, No. 5, pp. 468-475.

Brewster M.Q., and C.L. Tien, 1982, "Radiative Transfer in Packed Fluidized Beds: Dependent Versus Independent Scattering", *Journal of Heat Transfer*, Vol. 104, No. 4, pp. 573-579.

Byrd, R.H., M.E. Hribar, and J. Nocedal, 1999, "An Interior Point Algorithm for Large-Scale Nonlinear Programming", *SIAM Journal on Optimization*, Vol. 9, No. 4, pp. 877–900.

Daun K.J., H. Erturk, and J.R. Howell, 2002, “Inverse Methods for High Temperature Systems”, *Arabian Journal for Science and Engineering*, Vol. 27, No. 2C, pp. 3-48.

Duffie J.A., and W.A. Beckman, 2006, *Solar Engineering of Thermal Processes*, Wiley, Hoboken.

Etherden N., T. Tesfamichael, G.A. Niklasson, and E. Wackelgård, 2004, “A Theoretical Feasibility Study of Pigments for Thickness Sensitive Spectrally Selective Paints”, *Journal of Physics D: Applied Physics*, Vol. 37, pp. 1115-1122.

Granqvist C.G., 1985, “Spectrally Selective Coatings for Energy Efficiency and Solar Applications”, *Physica Scripta*, Vol. 42, pp. 401-407.

Hartel W., 1940, "Zur Theorie der Lichtstreuung Durch Trube Schichten Besonders Trubglaser", *Licht*, Vol. 10, pp. 141–143, 165, 190, 191, 214, 215, 232–234.

Hottel H.C., A.F. Sarofim, I.A. Vasalos, and W.H. Dalzell, 1970, “Multiple Scatter: Comparison of Theory with Experiment”, *Journal of Heat Transfer*, Vol. 92, No. 2, pp. 285-291.

Howell J.R., K.J. Daun, H. Erturk, M. Gamba and M. Sarvari, 2003, “The Use of Inverse Methods for Design and Control of Radiant Sources”, *JSME International Journal, Series B, Fluid and Thermal Engineering*, Vol. 46, pp. 470-478.

Howell J.R., R. Siegel, and M.P. Menguc, 2011, *Thermal Radiation Heat Transfer*, 5th ed., Taylor & Francis Group, London.

Jacobson, M.Z., and M.A. Delucci, 2009, “A Path to Sustainable Energy by 2030”, *Scientific American*, Vol. 301, pp. 59-65.

Jurisson J., R.E. Peterson, and H. Mar, 1975, “Principles and Applications of Selective Solar Coatings”, *Journal of Vacuum Science & Technology*, Vol. 12, pp. 1010-1015.

Kalogirou S.A., 2003, “Solar Thermal Collectors and Applications”, *Progress in Energy and Combustion Science*, Vol. 30, pp. 231-295.

Kazmerski L.L, 2004, “Photovoltaics R&D at the Tipping Point”, *DOE Solar Energy Technologies* , Denver, Colorado.

Kennedy C.E, 2002, Review of Mid to High Temperature Solar Selective Absorber Materials, NREL/TP-520-31267.

Lagarias J.C., J. A. Reeds, M. H. Wright, and P. E. Wright, 1998, “Convergence Properties of the Nelder-Mead Simplex Method in Low Dimensions”, *SIAM Journal of Optimization*, Vol. 9, No. 1, pp. 112-147.

Mackowski D.W., and M.I. Mishchenko, 2011, “A Multiple Sphere T-matrix Fortran Code for Use on Parallel Computer Clusters”, *Journal of Quantitative Spectroscopy & Radiative Transfer*, Vol. 112 , pp. 2182-2192.

Maheu B., J.N. Letoulouzan, and G. Gouesbet, 1984, “Four Flux Models to Solve the Scattering Transfer Equation in Terms of Lorentz-Mie Parameters”, *Applied Optics*, Vol.23, No. 19, pp. 3353-3362.

Mie G., 1908, “Beiträge Zur Optik Trüber Medien, Speziell Kolloidaler Metallösungen”, *Annalen der Physik*, Vol. 25, No. 3, pp. 377-445.

Niklasson G.A., 2006, “Modeling the Optical Properties of Nanoparticles”, *SPIE Newsroom*, Vol. 89, No. 9, pp. 2-4.

Nelder J.A., and R. Mead, 1965, “A Simplex Method for Function Minimization”, *Computation Journal*, Vol.7, pp. 308–313.

Oktik Ş., 2011, “*Güneş Enerjisi*”, Bilim ve Teknik, No. 523, pp. 44-49.

Peterson R.E., and J.W. Ramsey, 1975, "Thin Film Coatings in Solar Thermal Power Systems", *Journal of Vacuum Science and Technology*, Vol. 12, pp. 174-181.

Press W.H., S.A. Teukolsky, W.T. Vetterling, and B.P. Flannery, 1992, *Numerical Recipes in FORTRAN: The Art of Scientific Computing*, 2nd. edition, Cambridge University Press, Cambridge.

Siegel R., and J.R. Howell, 1992, *Solar Engineering of Thermal Processes*, 3rd. edition, Taylor & Francis, Washington.

Shockley W. and H.J. Queisser., 1961, "Detailed Balance Limit of Efficiency of P-N Junction Solar Cells", *Journal of Applied Physics*, Vol. 32, pp. 510-519.

Vargas W.E., and G.A. Niklasson, 1997a, "Pigment Mass Density and Refractive Index Determination from Optical Measurements", *Journal of Physics: Condensed Matter*, Vol. 9, pp. 1661-1670.

Vargas W.E., and G.A. Niklasson, 1997b, "Forward Scattering Ratios and Average Pathlength Parameter in Radiative Transfer Models", *Journal of Physics: Condensed Matter*, Vol. 9, pp. 9083-9096.

Vargas W.E., and G.A. Niklasson, 1997c, "Applicability Conditions of the Kubelka-Munk Theory", *Applied Optics*, Vol. 36, No. 22, pp. 5580-5586.

Vargas W.E., and G.A. Niklasson, 1997d, "Generalized Method for Evaluating Scattering Parameters Used in Radiative Transfer Models", *Journal of Optical Society of America*, Vol. 14, No. 9, pp. 2243-2252.

Vargas W.E., 1997, *Light Scattering and Absorption in Pigmented Coatings: Theory and Experiments*, Ph.D. Thesis, Uppsala University.

Vargas W.V., 1998, "Generalized Four Flux Radiative Transfer Model", *Applied Optics*, Vol. 37, No. 13, pp. 2615-2623.

Vargas W.V., E.M. Lushiku, G.A. Niklasson, and T.M.J. Nilsson, 1998, “Light Scattering Coatings: Theory and Solar Applications”, *Solar Energy Materials and Solar Cells*, Vol. 54, pp.343-350.

Vargas W.E., 2000, “Optimization of Diffuse Reflectance of Pigmented Coatings Taking into Account Multiple Scattering”, *Journal of Applied Physics*, Vol. 88, No. 7, pp. 4079-4084.

Vargas W.E., P. Greenwood, J.E. Otterstedt, and G.A. Niklasson, 2000, “Light Scattering in Pigmented Coatings: Experiments and Theory”, *Solar Energy*, Vol. 68, No. 6, pp. 553-561.

Vargas W.E, and G.A. Niklasson, 2001, “Reflectance of Pigmented Polymer Coatings: Comparisons between Measurements and Radiative Transfer Calculations”, *Applied Optics*, Vol. 20, No. 1, pp. 85-94.

Vargas W.E., 2003, “Optical Properties of Pigmented Coatings Taking into Account Particle Interactions”, *Journal of Quantitative Spectroscopy and Radiative Transfer*, Vol. 78, pp. 187-195.

Vidal J., 2005, *The End of Oil is Closer than You Think*, http://www.guardian.co.uk/science/2005/apr/21/oilandpetrol.news, accessed at February 2012.

Yalcin R.A., and H. Erturk, 2011, “Optimization of Pigmented Coatings for Concentrating Solar Thermal Systems", *Proceedings of 2011 International Mechanical Engineering Congress and Exhibition*, Denver, Co, USA.

Zhao S., and E. Wackelgard, 2006, “Optimization of Solar Absorbing Three Layer Coatings”, *Solar Energy Materials & Solar Cells*, Vol. 90, No. 40, pp. 243–261.